Stable Fe isotope fractionation during dissimilatory Fe(III) reduction by a thermoacidophile in acidic hydrothermal environments

Piyali Chanda[1,2*], Maximiliano J. Amenabar [2,3], Eric S. Boyd[2,3], Brian L. Beard[1,2], and Clark M. Johnson[1,2]

[1]Dept. of Geoscience, University of Wisconsin-Madison, WI, 53706, USA

[2] NASA Astrobiology Institute, Mountain View, CA, 94035, USA

[3]Dept. of Microbiology and Immunology, Montana State University, Bozeman, MT, 59717, USA

***Corresponding Author's current address:**

Piyali Chanda
School of Earth and Sustainability
Northern Arizona University
624 S Knoles Dr., Flagstaff, AZ, 86011, USA
Email: Piyali.Chanda@nau.edu
Ph. +1-732-668-1881

Keywords: Dissimilatory Fe reduction, stable Fe isotope fractionation, Fe isotope exchange, low-pH, thermoacidophiles, Archaea, biosignature

ABSTRACT

Dissimilatory iron reduction (DIR) plays an essential role in biogeochemical Fe cycling in anoxic environments. At near-neutral pH, in both biotic and abiotic systems, aqueous Fe(II) ($Fe(II)_{aq}$) interacts with reactive ferric (hydr)oxides via electron transfer and atom exchange that is catalyzed by large amounts of sorbed Fe(II). This may result in substantial Fe isotope exchange, which, at equilibrium, produces up to a ~4‰ $^{56}Fe/^{54}Fe$ fractionation between coexisting oxide/hydroxide and $Fe(II)_{aq}$, depending on mineralogy. The role of biology in such systems has been interpreted to lie in the production of Fe(II) rather than a specific "vital" effect, such as enzymatic and kinetic processes. Under acidic abiotic conditions, however, the lack of sorbed Fe(II) generates little Fe isotope exchange, and, by extension, it has been expected that little exchange would occur during DIR at low pH if sorbed Fe(II) is the key component for catalyzing isotopic exchange.

In this study, we explored the extent and mechanism of Fe isotope exchange between $Fe(II)_{aq}$ and ferric hydroxides (ferrihydrite and goethite), including determination of the $^{56}Fe/^{54}Fe$ fractionations during DIR by *Acidianus* strain DS80 at pH ~3.0 and 80°C, over 19 days of incubation. Significant Fe(III) reduction occurred for both minerals along with large changes in Fe isotope compositions for $Fe(II)_{aq}$, indicating Fe isotope exchange. Solid-phase extractions using HCl confirmed a lack of sorbed Fe(II), which suggests that a mechanism other than sorption is required to catalyze Fe isotope exchange during DIR at low pH. Reactive Fe(III) ($Fe(III)_{reac}$) extracted from the mineral surface allowed for the calculation of the Fe pools that underwent isotopic exchange. A total of ~20% of goethite and ~60% of ferrihydrite underwent isotopic exchange over 19 days. For goethite from biotic experiments, we calculate a $Fe(III)_{reac}$-$Fe(II)_{aq}$ fractionation factor of 1.57±0.52‰, which is larger than the abiotic equilibrium fractionation factor (~0.73‰ at 80°C). This result is consistent with previous work on DIR of goethite at neutral pH, where a fractionation factor larger than equilibrium was interpreted to reflect an isotopically distinct “distorted surface layer” of goethite produced during exchange with $Fe(II)_{aq}$. In contrast to goethite, the difference between the $Fe(III)_{reac}$-$Fe(II)_{aq}$ fractionation factor for ferrihydrite from our biotic reactors (2.91±0.40‰) and the abiotic equilibrium fractionation factor (~2.28‰ at 80°C, under silica-free conditions) is smaller.

Ultimately, the contrast in the extent of Fe isotope exchange between biotic and abiotic experiments emphasizes the importance of biology in promoting Fe isotope exchange in acidic systems. We speculate that the unique role of biology at low pH in catalyzing Fe isotope exchange, not seen in equivalent abiotic systems, must lie in the transport of electrons to the ferric hydroxide surface that produces Fe(II) atoms *in situ*. This suggests that isotopic exchange occurs on an atom-by-atom basis as Fe(III) is reduced to Fe(II), followed by the release of Fe(II) into solution. This study demonstrates that significant variations in Fe isotope compositions may be uniquely produced in acidic

environments where microbial Fe cycling occurs via DIR, compared to minor isotopic variations observed previously in acidic abiotic systems.

1. INTRODUCTION

Dissimilatory iron reduction (DIR) is considered as one of the earliest forms of respiration (Vargas et al., 1998). Diverse groups of microorganisms (Bacteria and Archaea) perform DIR, generating energy by coupling reduction of Fe(III) (in both solid and dissolved forms) to the oxidation of organic matter or H_2 (Vargas et al., 1998; Lloyd, 2003; Lovley et al., 2004; Weber et al., 2006). Consequently, DIR is recognized as an important biogeochemical process responsible for Fe cycling in anoxic modern and ancient environments (Amenabar and Boyd, 2019). Stable Fe isotope fractionation during DIR involving various ferric (hydr)oxides at near-neutral pH and room temperature has been studied extensively in both experimental and natural systems (Beard et al., 1999; Beard et al., 2003; Icopini et al., 2004; Crosby et al., 2005; Johnson et al., 2005; Crosby et al., 2007; Tangalos et al., 2010; Percak-Dennett et al., 2011). Substantial equilibrium Fe isotope fractionation (~2 to 4‰) occurs between ferric (hydr)oxides and dissolved Fe(II), dependent on mineralogy, where the $^{56}Fe/^{54}Fe$ ratios of soluble Fe(II) are always lower than the initial ferric (hydr)oxide substrates.

The majority of research on DIR has focused on understanding the mechanism(s) of iron oxide reduction by mesophilic bacteria such as *Geobacter* spp. and *Shewanella* spp. under near-neutral pH (e.g., Lovley et al., 2004; Nealson and Scott, 2006; Shi et al. 2007; Fredrickson et al., 2008; Shi et al., 2009). This approach has been mirrored in experimental studies of Fe isotope fractionation during DIR (e.g., Beard et al., 1999; Beard et al., 2003; Icopini et al., 2004; Crosby et al., 2005; Johnson et al., 2005; Crosby et al., 2007; Percak-Dennett et al., 2011). Recently, a few studies have documented DIR in thermoacidophilic Archaea, including a variety of members of the genus *Acidianus* within the order Sulfolobales. For example, *Acidianus* strain DS80 was shown to couple H_2 or S^0 oxidation with reduction of soluble or solid phase Fe(III) (Amenabar et al., 2017; Amenabar and Boyd, 2018). Solid phase Fe(III) that supported DIR in this taxon included ferrihydrite, goethite, and hematite. Intriguingly, growth and DIR activity with ferrihydrite was documented with and without direct contact between cells and the mineral surface (Amenabar and Boyd, 2018), although the rate of DIR differs between these two conditions. Microscopic evidence that *Acidianus* cells are not attached to ferrihydrite grains, even when provided with direct access to the mineral, suggests that cells likely reduce dissolved Fe(III) ions, which are leached out from ferrihydrite in acidic pH or by dissolution promoted by cells.

The primary mechanism for Fe isotope fractionation during DIR has been proposed to be coupled electron transfer and Fe atom exchange between dissolved Fe(II) and solid Fe(III) (Crosby et al., 2005, 2007). According to this model, at neutral pH,

115 sorption of significant amounts of aqueous Fe(II) onto Fe(III)-oxide surfaces catalyzes
116 electron transfer, which in turn promotes Fe atom (isotopic) exchange, thereby producing
117 significant $^{56}Fe/^{54}Fe$ fractionation between Fe(III)-oxide/hydroxides and aqueous Fe(II).
118 The work by Reddy et al. (2015) at low pH (~2.5), however, indicates that the very
119 limited sorption of Fe(II) onto Fe(III) hydroxides (goethite) under acidic conditions
120 results in negligible Fe isotope exchange. In this contribution, we experimentally
121 investigated the extent of stable Fe isotope exchange and fractionation during DIR of
122 nanoparticulate ferric hydroxides by *Acidianus* strain DS80 at low pH. Although the
123 abiotic experiments by Reddy et al. (2015) suggest that limited Fe isotope exchange
124 might be expected at low pH, we find significant isotopic exchange and large $^{56}Fe/^{54}Fe$
125 fractionations between aqueous Fe(II) and two different Fe(III)-oxides (i.e., ferrihydrite
126 and goethite) during growth of DS80 at pH ~3.0 and 80°C. These observations clearly
127 show the contrast between abiotic and biotic systems at low pH as compared to near-
128 neutral pH, and the results are discussed in light of the potential utility of Fe isotopes as a
129 biosignature of microbial activity in acidic terrestrial and extra-terrestrial environments.
130
131 **2. MATERIALS AND METHODS**
132
133 **2.1. Fe reduction experiments with thermoacidophiles and ferric (hydr)oxides**
134 Microbial Fe(III) reduction by *Acidianus* strain DS80 at low pH was
135 experimentally investigated over 19 days using two different substrates, ferrihydrite and
136 goethite. This particular strain was previously isolated by authors Amenabar and Boyd
137 from an acidic hot spring ("Dragon Spring", Yellowstone National Park (YNP) thermal
138 inventory ID: NHSP042), located in the Norris Geyer Basin (44° 43' 55" N, 110° 42' 39"
139 W) at YNP, Wyoming, USA (Amenabar et al., 2017). Following growth of the culture on
140 H_2 and S^0 to log phase, cells were subjected to a low spin concentration (5000 g, 5 min.,
141 25°C) to separate cells from S^0. The supernatant was then concentrated using a 0.22 μm
142 filter, and filtered cells were washed with anoxic sterile growth medium (base salts
143 mineral medium; see Table S.1; Supplementary Material) to remove dissolved sulfide.
144 The filtered cells were then transferred to an evacuated serum bottle containing anoxic
145 sterile growth medium without trace elements and vitamin solutions under a stream of N_2
146 gas. This cell suspension was then used as the inoculum for the DIR experiments. No
147 detectable sulfide or iron was present in the inoculum. The stock minerals, ferrihydrite
148 and goethite, were synthesized aseptically using sterilized reagents according to methods
149 described previously (Lovley and Phillips, 1986) and were characterized for mineralogy
150 and surface area using X-Ray Diffraction (XRD), Field Emission Scanning Electron
151 Microscopy (FE-SEM), and Brunauer-Emmett-Teller (BET) surface area analyzer (see
152 Supplementary Material). The specific surface area of stock ferrihydrite and goethite are

386.7 m^2/g and 95.3 m^2/g, respectively. XRD analyses confirmed that the two stock minerals were exclusively ferrihydrite and goethite.

Forty reactors were prepared with acid-cleaned (10% nitric acid) 160 ml borosilicate glass serum bottles under anoxic conditions. Each reactor contained 58 ml of growth medium (pH 2.9) that had been subjected to autoclave sterilization. Following autoclave sterilization, filter sterilized (0.22 μm) Wolfe's vitamins (1 ml l^{-1} final concentration (Atlas, 1997)), and filter sterilized (0.22 μm) SL-10 trace metals (1 ml l^{-1} final concentration (Widdel et al., 1983)) that lacked added iron were each added to the reactors while they were still hot (~90°C), as described previously (Boyd et al., 2007). All reagents used to prepare Wolfe's vitamins and SL-10 trace metals were of American Chemical Society grade or higher. Prior to addition of trace metals and vitamins, an equal volume of culture medium was removed to maintain the solution volume at 58 ml. Twenty reactors were provided with 0.0139 ± 0.0005 g of ferrihydrite and the rest of the reactors were provided with 0.0136 ± 0.0001 g of goethite. After addition of ferric hydroxides, the pH of the medium increased slightly (to ~3.03-3.09 for ferrihydrite and to ~2.98-3.00 for goethite). Following nutrient amendments, serum bottles and their contents were deoxygenated by purging with O_2-free, sterile N_2. The serum bottles were then sealed with butyl rubber stoppers and heated to 80°C followed by replacement of the headspace with a H_2-CO_2 gas mixture (80%: 20%, vol./vol.). Thirty reactors containing each type of substrate (15 with goethite and 15 with ferrihydrite) were amended with 2 ml of inoculum to initiate the experiment. The remaining reactors were used as abiotic controls for each substrate where, instead of adding the inoculum, 2 ml of sterile deoxygenated growth medium was added. Finally, all reactors, each containing 60 ml of solution, were incubated at 80°C and subsequently sampled at five time points (i.e., 2, 4, 6, 10, and 19 days). At each time point, three biotic reactors and one abiotic reactor for each substrate were sacrificed. All growth experiments were conducted at Montana State University (MSU).

2.2. Procedures for sampling, extraction, and Fe concentration analysis

Reactors were sacrificed at designated sampling points to avoid mass-balance changes that would occur if a single large reactor was successively sampled. Therefore, each reactor must be considered a unique experiment, although we attempted to make each reactor identical to the extent possible. Although this approach is required to avoid mass-balance changes, it does mean that there may be some variability in microbial activity between reactors, which may produce different reduction and isotopic exchange kinetics. The solid and fluid components at the time of sampling were separated via a two-step centrifugation method. Briefly, the contents of each reactor were centrifuged at 5000 g for ~10 minutes at 4°C to separate the solid and aqueous phases. The aqueous phase was transferred to sterile acid-cleaned polypropylene vial and the solids were

192 subjected to a second centrifugation step at 14,000 g for ~1 minute at 4°C to separate any
193 remnant fluids from the solids. The solids from each reactor were also rinsed with the
194 anoxic sterile growth medium to remove any pore fluid that might contain dissolved Fe.
195 The solids were transferred to sterile acid-cleaned polypropylene vials that were placed in
196 N_2-purged serum bottles; bottles and their contents were stored at 4°C prior to analysis.
197 The aqueous phase obtained after the first and second centrifugation steps were collected,
198 filtered (0.22 μm), and stored in sterile N_2-purged and acid-washed (10% nitric acid) 160
199 ml borosilicate glass serum bottles at 4°C. The pH and concentration of Fe(II) and total
200 Fe in the aqueous phase (*Ferrozine* assay; Stookey, 1970), were determined following
201 methods described by Amenabar et al. (2017). The serum bottles were sealed within an
202 anaerobic chamber and these were shipped to the University of Wisconsin-Madison
203 (UW) for further processing and Fe isotope analysis.

204 All samples were stored inside an anaerobic chamber at UW and concentrations
205 of Fe(II) and total Fe in the solutions were re-analyzed to ensure that samples were not
206 oxidized or contaminated during shipping and handling. Iron measurements performed at
207 MSU and the UW were calibrated using the same set of Fe standards and the Fe
208 concentration obtained at UW were very similar to the data collected at MSU within
209 analytical uncertainty (± 10%, Table S.2; Supplementary material). The solids from two
210 biotic reactors and one abiotic reactor from each time point were treated with ~2 ml of
211 HCl solution (10 mM HCl for ferrihydrite and 1 M HCl for goethite) at 60°C for 1 hour
212 to extract Fe(II) in the solid, as well as leachable Fe(III). Based on prior work, such
213 leaches appear to target reactive Fe(III) that underwent Fe isotope exchange, and might
214 be envisioned as the outer layers of Fe(III) hydroxides (e.g., Crosby et al., 2005, 2007).
215 Because of the different solubility and reactivity of the Fe oxides used in this study,
216 different molarities of HCl solutions were chosen so that the mass of extracted Fe from
217 the minerals would be sufficient for Fe isotope analysis, but simultaneously be as small
218 as possible to facilitate isolating reactive Fe(III) components from the bulk "unreacted"
219 solids. Afterwards, the samples were centrifuged and the supernatants (i.e., HCl
220 solutions) were separated from solid residues via pipetting, followed by passing through
221 0.22 μm filters and complete dissolution of solid residues in 2 M HCl. The whole
222 extraction and digestion procedure was conducted inside an anaerobic chamber to prevent
223 oxidation of Fe(II) components. The post-experiment solids from the remaining reactors
224 (i.e., one from each time point) were evaporated at room temperature using a desiccator
225 inside an anaerobic chamber and examined using an XRD and an FE-SEM to confirm
226 their mineralogy.

227 The concentrations of Fe(II) and total Fe of solution, extracted Fe, and digested
228 solid residues were analyzed using a spectrophotometer following the *Ferrozine* method
229 (Stookey, 1970), which was slightly modified by adding ~50 μL of 0.1M NH_4F to each
230 sample prior to treatment with *Ferrozine* buffer to prevent any interference from Fe(III)
231 ions on the Fe adsorption spectra (Krishnamurti and Huang, 1990). The concentration of

Fe(III) in samples was determined by the difference between the measured concentrations of total Fe and Fe(II). Uncertainties in concentration measurements were determined from the errors of measured absorbance and sample weight. The detection limit for analyzing Fe concentration using the *Ferrozine* method was ~1.8 μM. The total mass of Fe recovered from solution, HCl-extract, and residual solid from each reactor confirmed that mass balance was maintained for our experiments (~100±3%, Table S.3; Supplementary Material).

2.3. Ion-exchange chromatography and Fe isotope analysis

The three different components sampled from each reactor, i.e., (i) aqueous Fe, (ii) HCl-extracted Fe, and (iii) Fe from dissolved solid residue, were dried and treated with concentrated HNO_3 and 30% H_2O_2 to remove organic matter. Afterwards, the ion-chromatographic purification of Fe from these samples was conducted using anion-exchange resin columns (Bio-Rad AG 1-X4 200–400 mesh) following the previous method (Beard et al., 2003). Concentrations of Fe in samples before and after anion-exchange chromatography were determined using the *Ferrozine* method (Stookey, 1970) to ensure near-quantitative recovery of Fe (98 ± 5%). Following chemical purification, Fe isotopes ($^{56}Fe/^{54}Fe$ and $^{57}Fe/^{54}Fe$) of these samples were analyzed using a *Nu Plasma II* MC-ICP-MS. Purified Fe solutions were diluted to 600 ppb in 0.1% HNO_3 and analyzed following the dry plasma method (Cetac Aridus II with ~50 μl/min Savillex desolvating nebulizer) using a 100 μm-wide defining slit. This technique allowed measurement of intensities of ^{54}Fe, ^{56}Fe, and ^{57}Fe peaks that were free from polyatomic interferences (e.g., $^{40}Ar^{14}N$, $^{40}Ar^{16}O$, and $^{40}Ar^{16}OH$) (Weyer and Schwieters, 2003). We also simultaneously monitored the ^{53}Cr signal, and we applied the ^{54}Cr-correction on the measured ^{54}Fe intensity when ^{53}Cr signal was $>5\cdot10^{-5}$ volts (10^{11} Ω resistor). However, this Cr-correction was only required for a very few samples (~3% of total samples analyzed) and the magnitude of correction was ≤0.1‰. A sample-standard bracketing technique was utilized to correct for instrumental mass bias on Fe isotope data during analytical sessions.

Stable Fe isotope compositions are reported using standard delta (δ) notation in units of per mil (‰):

$$\delta^{56}Fe = \left[\frac{(^{56}Fe/^{54}Fe)_{sample}}{(^{56}Fe/^{54}Fe)_{standard}} - 1\right] \cdot 1^{3} \qquad \text{----Eq.1}$$

The average $^{56}Fe/^{54}Fe$ ratio of igneous rocks is used as the reference standard. On this scale, the $\delta^{56}Fe$ value of pure in-house standards, UW HPS Fe, IRMM-14, and UW J-M Fe were 0.49 ± 0.08‰, -0.08 ± 0.09‰, and 0.25 ± 0.07‰, respectively (2 standard deviation; n = 25) that are similar to published values (Table S.4, Supplementary Material). The precision and accuracy of the Fe isotope analyses were assessed using

multiple analyses of pure Fe standards (UW HPS Fe, IRMM-14, and UW J-M Fe), as well as test solutions prepared using matrices similar to the growth medium and HCl solutions used in the incubation experiments and extraction procedures, respectively. Each test solution contained Fe of known isotopic composition in the same mass proportions as present in the sample matrix (Table S.5; Supplementary Material). Collectively, these tests show that the analytical uncertainty (i.e., 2 times the standard deviation) of δ^{56}Fe values is ±0.08‰.

In addition, initial Fe(III) hydroxides were partially leached using HCl solutions (see section 2.2) and analyzed for Fe isotopes to evaluate isotopic homogeneity of the solids. The one-hour partial HCl extraction using 10 mM HCl dissolved ~0.15% Fe from ferrihydrite, and 1 M HCl dissolved ~1% Fe from goethite. The similarity of δ^{56}Fe values between initial bulk solid, HCl-extracted Fe, and residue Fe for each mineral confirmed that the solid substrates used for the incubation experiments were isotopically homogeneous (Table S.6; Supplementary Material).

The mass-dependent Fe isotope fractionation factor between two coexisting phases (X and Y) is expressed using the standard notation:

$$\Delta^{56}Fe_{X-Y} = \delta^{56}Fe_X - \delta^{56}Fe_Y \approx 1^{3} \cdot ln\alpha^{56}_{X-Y} \quad \text{----Eq.2}$$

Here α^{56}_{X-Y} is the ratio of ^{56}Fe/^{54}Fe between phases X and Y.

3. RESULTS

We first focus on temporal changes in the measured chemical and isotopic compositions of the solids, fluids, and leaches. These parameters describe changes in the reactive Fe pools, both in terms of pool sizes and Fe isotope fractionations, and this discussion is followed by a description of the calculations that are used to infer these quantities. Definitions of measured and derived parameters are listed in Table 1.

3.1. Concentration and speciation of Fe in solutions and solids during Fe(III) reduction

Cultures of *Acidianus* strain DS80, provided with H_2 as the electron donor and ferrihydrite or goethite as the electron acceptor, showed a maximum of ~218 μM and ~430 μM increase in total aqueous Fe ($Fe_{aq, tot}$) during 19 days of incubation, respectively (Figure 1A and B, Table 2). In contrast, the increase in $Fe_{aq, tot}$ in abiotic reactors with both minerals was negligible (i.e., ~20 and ~21 μM for ferrihydrite and goethite, respectively) over the same duration. In biotic experiments, the $Fe_{aq, tot}$ was primarily Fe(II) for both minerals except the last sampling point (day 19), where an increase in dissolved Fe(III) was detected (Figure 1C and D, Table 2). Cultures provided with

ferrihydrite showed that the $Fe_{aq, tot}$ comprised a maximum of ~25% Fe(III), whereas cultures provided with goethite showed a maximum of ~35% of $Fe_{aq, tot}$ as Fe(III). In comparison, no significant amounts of Fe(III) were detected in the $Fe_{aq, tot}$ obtained from the abiotic reactors (Figure 1C and D, Table 2). The pH of the solutions from the biotic reactors increased slightly (~0.2 pH unit) over 19 days, regardless of the substrate, whereas the pH of solutions from abiotic reactors remained constant over time (Table 2).

Partial leaching of residual substrates after incubation using HCl resulted in extraction of a small fraction of Fe (i.e., <0.25% Fe from ferrihydrite and <1.2% Fe from goethite) (Figure 2A and B). The HCl-extracted Fe ($Fe_{extracted}$) from the biotic reactors was primarily comprised of Fe(III) with a minor amount of Fe(II) (ferrihydrite: ~6-23%; goethite: ~3-15%) (Figure 2C and D, Table 3). The $Fe_{extracted}$ from abiotic reactors containing ferrihydrite and goethite was also mostly Fe(III), with a small amount of Fe(II) (~4.7-10.7% and ~3.0%, respectively). The Fe in the residual solids ($Fe_{residue}$) after HCl-extraction was almost entirely Fe(III) (Table 3).

The extent of Fe reduction, expressed as "% Fe reduction", is calculated from the measured total moles of Fe(II) present in each reactor (i.e., solution+solid) for a given time point relative to the initial moles of Fe(III) provided to that reactor. In biotic reactors, the initial % Fe reduction was ~1% (~day 2), which increased up to ~6% (ferrihydrite) and ~11% (goethite) over 19 days (Figure 3). In contrast, the temporal variability in % Fe reduction in abiotic reactors was very small (between ~0.5 to 0.8%) for both ferric hydroxide substrates.

3.2. Fe isotope compositions of solutions and solids during reduction of ferric hydroxides

The measured Fe isotope compositions of solutions, solids, and extracted Fe are summarized in Table 4 and Figure 4. In biotic experiments with ferrihydrite, following two days of incubation, the $\delta^{56}Fe$ value of total aqueous Fe ($\delta^{56}Fe_{aq, tot}$) was ~ -2.60‰, which increased by ~0.5‰ over 19 days, approaching the $\delta^{56}Fe$ value of the bulk solids (~0.05‰) (Figure 4A). The $\delta^{56}Fe$ values of $Fe(II)_{aq}$ were calculated assuming isotopic equilibrium was maintained between coexisting $Fe(II)_{aq}$ and $Fe(III)_{aq}$, as justified by the rapid isotope exchange kinetics between these species (Welch et al., 2003), using the following equation (Eq.3):

$$\delta^{56}Fe_{Fe(II)_{aq}} = \delta^{56}Fe_{aq,tot} - \frac{M_{Fe(III)_{aq}}}{M_{Fe_{aq}}} \cdot \Delta^{56}Fe_{Fe(III)_{aq}-Fe(II)_{aq}} \quad \text{----Eq.3}$$

Here, the fractionation factor between aqueous Fe(III) and Fe(II) (i.e., $\Delta^{56}Fe_{Fe(III)_{aq}-Fe(II)_{aq}}$) is assumed to be +2.87‰ at 22°C and 11 mM Cl^- concentration, (Welch et al., 2003), which most closely matches our experimental conditions, where the aqueous Fe had equilibrated at room temperature after separation from the reactors and

had a Cl^- concentration of ~15 mM. The terms $M_{Fe(III)_{aq}}$ and $M_{Fe_{aq}}$ represent total moles of aqueous Fe(III) and aqueous total Fe, respectively. Calculated $\delta^{56}Fe$ values for $Fe(II)_{aq}$ remained identical to the measured $\delta^{56}Fe_{aq,\,tot}$ values, except the reactors sampled at day 19, where $Fe_{aq,\,tot}$ consisted of ~20% Fe(III). Despite slight variability (± 0.3‰), the $\delta^{56}Fe$ values of total Fe in both HCl-extracts (i.e., $\delta^{56}Fe_{extracted}$) and solid residues ($\delta^{56}Fe_{residue}$) from the ferrihydrite-bearing biotic experiments remained similar to the initial bulk solid $\delta^{56}Fe$ (~0.05‰) (Figure 4A). Similarly, in biotic experiments with goethite, the $\delta^{56}Fe_{aq,\,tot}$ value increased by ~0.9‰ over time (i.e., -1.09‰ at day 2 to -0.16‰ at day 19), approaching the initial bulk solid $\delta^{56}Fe$ (~0.01‰). However, unlike ferrihydrite, in goethite-containing experiments the $\delta^{56}Fe_{extracted}$ was higher (0.4 to 0.8‰) than the $\delta^{56}Fe_{residue}$ (0.03 ± 0.05‰), the latter of which was similar to the initial bulk solid $\delta^{56}Fe$ value (Figure 4B).

In contrast to the biotic experiments, the $\delta^{56}Fe_{aq,\,tot}$ value in abiotic reactors with ferrihydrite remained mostly constant at -2.60‰ during the experimental period, except the 4th sampling time point (i.e., day 10), where the $\delta^{56}Fe_{aq,\,tot}$ value was slightly higher (-2.12‰). The $\delta^{56}Fe_{extracted}$ and the $\delta^{56}Fe_{residue}$ values from abiotic reactors remained close to the initial bulk solid $\delta^{56}Fe$ (~0.05‰) (Figure 4C). In abiotic reactors with goethite, the $\delta^{56}Fe_{aq,\,tot}$ value decreased slightly from -1.19‰ to -1.58‰ over 19 days. The $\delta^{56}Fe_{residue}$ value (0.03 ± 0.10‰) from these abiotic reactors was similar to the initial bulk goethite $\delta^{56}Fe$ (~0.01‰). However, values of the $\delta^{56}Fe_{extracted}$ were higher (~0.4 to 0.6‰) than the $\delta^{56}Fe$ values of both $Fe_{residue}$ and initial bulk goethite (Figure 4D).

3.3. Comparison between pre- and post-incubation solids

High-resolution FE-SEM images of the pre- and post-incubation solids (Figure 5) showed no obvious changes in morphology of mineral grains for either ferrihydrite or goethite over 19 days. However, subtle differences between stock ferrihydrite and post-incubation ferrihydrite were observed (Figure 5A and C), where grains in post-incubation solids are more well-defined and smaller when compared to the pre-incubation ferrihydrite. Importantly, however, there is no evidence of significant new mineral formation and the solid phase remained entirely ferrihydrite following incubation. The XRD spectra collected from pre- and post-incubation ferrihydrite also looked very similar, suggesting that ferrihydrite remained mostly amorphous during the experiment (Figure S.1A, Supplementary Material). Slight differences observed between the XRD patterns from pre- and post-incubation ferrihydrite might reflect minor secondary remineralization to nanoparticulate lepidocrocite, although the extent of mineralogical transformation of ferrihydrite was not at all pervasive considering ~1 wt. % as the detection limit of the XRD technique. The XRD spectra collected from pre- and post-incubation goethite also showed no detectable changes in mineralogy or crystallinity during DIR (Figure S.1B, Supplementary Material). In no case was there evidence of production of new crystalline Fe(II)-bearing minerals such as magnetite.

3.4. Calculation of δ^{56}Fe values of Fe(II) and Fe(III) end-members in extracted Fe and determination of the ^{56}Fe/^{54}Fe fractionation factors

The HCl-extracted Fe from ferrihydrite and goethite represented a mixture of Fe(II) and Fe(III), where Fe(III) was the predominant species. Here we assume that the small amount of Fe(II) observed in HCl-extracted Fe was sorbed Fe(II). The justification for this assumption is discussed in detail in Section 4.2. The Fe(III) in the HCl extraction is interpreted to reflect acid dissolution of the Fe(III)-hydroxide substrate. It is possible that the Fe(III) in the HCl extraction is a mixture of Fe(III) dissolved from the surface reactive layer that underwent isotopic exchange and the underlying "unreacted" bulk substrate (i.e., substrate that did not undergo Fe isotope exchange). Importantly, the HCl-extraction only removed ≤1% of the substrate Fe, and >20% of the Fe atoms in nanoparticulate ferrihydrite and goethite reside in the surface layer (Handler et al., 2009; Beard et al., 2010; Wu et al., 2011; Hiemstra, 2013). Therefore, it is reasonable to assume that the Fe(III) in HCl-extractions mostly sampled the outer reactive Fe(III) layer of the mineral substrate (i.e., $Fe(III)_{reac}$). Thus, the $\delta^{56}Fe_{extracted}$ values (Table 4) reflect isotopic mixing between the $Fe(II)_{sorbed}$ and $Fe(III)_{reac}$, and the $\delta^{56}Fe(III)_{reac}$ values (Table 5) can be calculated from the measured $\delta^{56}Fe_{extracted}$ values using the following isotopic mass balance equation (Eq.4):

$$\delta^{56}Fe_{Fe(III)_{reac}} = \frac{1}{\left(1-X_{Fe(II)_{extracted}}\right)} \cdot \left[\delta^{56}Fe_{extracted} - X_{Fe(II)_{extracted}} \cdot \delta^{56}Fe_{Fe(II)_{extracted}}\right] \quad \text{----Eq.4}$$

Here, $X_{Fe(II)_{extracted}}$ and $\delta^{56}Fe_{Fe(II)_{extracted}}$ represent the molar fraction and isotopic composition of the Fe(II) end-member in the HCl-extracted Fe, respectively, which can be assumed as the sorbed Fe(II) in this case. Given that sorption of Fe(II) on oxide surfaces at pH~3 is unfavorable (Reddy et al., 2015), we expected very small amounts of sorbed Fe(II) in this study and we did not attempt to measure $\delta^{56}Fe_{Fe(II)_{sorbed}}$ directly. Instead, we indirectly estimated the values of $\delta^{56}Fe_{Fe(II)_{sorbed}}$ from the $\delta^{56}Fe_{Fe(II)_{aq}}$ values using the fractionation factors between $Fe(II)_{aq}$ and $Fe(II)_{sorbed}$ (i.e., $\Delta^{56}Fe_{Fe(II)_{sorbed}-Fe(II)_{aq}}$) for the respective minerals. Previous experiments have determined the $\Delta^{56}Fe_{Fe(II)_{sorbed}-Fe(II)_{aq}}$ fractionations at room temperature to be +0.8‰ and +1.24‰ for ferrihydrite and goethite, respectively (Beard et al., 2010; Wu et al., 2011). Because our experiments were conducted at 80°C, we extrapolated the $Fe(II)_{sorb}$-$Fe(II)_{aq}$ fractionation factors to 80°C (ferrihydrite: +0.56‰; goethite: +0.87‰) using a $\Delta^{56}Fe_{Fe(II)_{sorbed}-Fe(II)_{aq}}$ versus $10^6/T^2$ plot, assuming a zero fractionation at infinite

temperature. The isotopic mixing relation between the Fe(II) and Fe(III) end-members of the $Fe_{extracted}$ and the linear extrapolations to calculate the values of $\delta^{56}Fe_{Fe(III)_{reac}}$ are presented in Figure S.2 (Supplementary Material). The calculated values of $\delta^{56}Fe_{Fe(III)_{reac}}$ range from ~0.15‰ to 0.51‰ for ferrihydrite and ~0.46‰ to ~0.86‰ for goethite (Table 5). The uncertainties on the $\delta^{56}Fe_{Fe(III)_{reac}}$ values are estimated from analytical errors of the Fe(II) concentration and the measured $\delta^{56}Fe_{extracted}$.

The $^{56}Fe/^{54}Fe$ fractionation factor was calculated between the outer reactive Fe(III) layer (i.e., $Fe(III)_{reac}$) of ferric hydroxides and the $Fe(II)_{aq}$ using the following equation:

$$\Delta^{56}Fe_{Fe(III)_{reac}-Fe(II)_{aq}} = \delta^{56}Fe_{Fe(III)_{reac}} - \delta^{56}Fe_{Fe(II)_{aq}} \quad \text{----Eq.5}$$

The $\Delta^{56}Fe_{Fe(III)_{reac}-Fe(II)_{aq}}$ fractionations determined from experiments with ferrihydrite ranged from 2.49‰ to 2.96‰ in abiotic reactors and from 2.53‰ to 3.23‰ in biotic reactors. Experiments with goethite showed a slightly different range of $\Delta^{56}Fe_{Fe(III)_{reac}-Fe(II)_{aq}}$ values, which varied from 1.64‰ to 2.23‰ in abiotic reactors and 1.20‰ to 1.97‰ in biotic reactors (Figure 6, Table 5). The uncertainties of calculated fractionation factors were determined by propagating the 2 standard deviations of the calculated $\delta^{56}Fe$ values of $Fe(III)_{reac}$ and $Fe(II)_{aq}$.

3.5. The relative proportion of reactive Fe(III) in the system: a key parameter for Fe isotope exchange

Although both biotic and abiotic experiments show Fe isotope fractionation between $Fe(II)_{aq}$ and $Fe(III)_{reac}$, it is important to note that this does not indicate the size of the Fe pools that underwent isotopic exchange. This latter parameter reflects the "vigor" to which microbial reduction may catalyze Fe atom exchange relative to abiotic conditions, and this cannot be estimated through simple inspection of the isotopic fractionations between biotic and abiotic experiments. The total reactive Fe in each reactor can be described by the combination of three components: $Fe(II)_{aq}$, Fe(II) in the solid (≈ $Fe(II)_{sorbed}$), and $Fe(III)_{reac}$. The summation of Fe isotope compositions of individual components weighted by their relative mass fractions represents the isotopic composition of the reactive Fe, which is set to be equal to the Fe isotope composition of the initial ferric hydroxide substrate (defined as $\delta^{56}Fe_{sys}$) for isotopic mass balance. The total mass of $Fe(III)_{reac}$ can be defined by the sum of Fe(III) recovered in the $Fe_{extracted}$ and the remaining reactive Fe(III) in the solid residue that were not sampled during the HCl-extraction but that is required to satisfy the isotopic mass balance of the system. Given that the $\delta^{56}Fe_{sys}$ is close to 0‰ (ferrihydrite: ~0.05‰, goethite: ~0.01‰), an estimation of

461 the total moles of Fe(III)$_{reac}$ ($M_{Fe(III)_{reac}}$) in the reactive Fe system is performed using the
462 isotopic mass balance of the system (Eq.6), which is adapted from a previously described
463 equation by Crosby et al. (2007):

464

465 $$M_{Fe(III)_{reac}} = \frac{-\delta^{56}Fe_{Fe(II)_{aq}} \cdot M_{Fe(II)_{aq}} - \delta^{56}Fe_{Fe(II)_{sorbed}} \cdot M_{Fe(II)_{sorbed}}}{\delta^{56}Fe_{Fe(II)_{aq}} + \Delta^{56}Fe_{Fe(III)_{reac}-Fe(II)_{aq}}}$$ ---- Eq.6

466

467 Here, $M_{Fe(II)_{aq}}$ and $M_{Fe(II)_{sorbed}}$ represent moles of Fe(II)$_{aq}$ and Fe(II)$_{sorbed}$ present in the
468 system, respectively. The moles of Fe(II)$_{sorbed}$ is equivalent to the total moles of Fe(II)
469 present in HCl-extracts and in solid residues. The fractionation factors, i.e.,
470 $\Delta^{56}Fe_{Fe(III)_{reac}-Fe(II)_{aq}}$, are derived from the measured data using Eq.5 (Table 5).

471 The mole fraction of total reactive Fe(III) relative to the total Fe in the system
472 ($X_{Fe(III)_{reac}}$) is the key quantity that shows the size of the pool of Fe that underwent
473 isotopic exchange, and is estimated using the calculated values of $M_{Fe(III)_{reac}}$ and the
474 measured moles of Fe(III) in the solution (i.e., $M_{Fe(III)aq}$):

475

476 $$X_{Fe(III)_{reac}} = \frac{M_{Fe(III)reac} + M_{Fe(III)aq}}{M_{Total\,Fe_{system}}}$$ ---- Eq.7

477

478 A major observation in our study is that in biotic reactors, $X_{Fe(III)_{reac}}$ in solids increased
479 as a function of %Fe reduction (Figure 7). Over 19 days, the fraction of Fe(III)$_{reac}$ in the
480 solids appeared to be significantly higher during DIR involving ferrihydrite
481 ($X_{Fe(III)_{reac}}$~0.52-0.62) compared to that involving goethite ($X_{Fe(III)_{reac}}$~0.18-0.19). In
482 contrast, abiotic reactors showed only a small fraction of Fe(III)$_{reac}$ ($X_{Fe(III)_{reac}}$ ~0.09 and
483 ~0.02 for ferrihydrite and goethite, respectively) (Figure 7). This highlights a major
484 difference in the size of the exchangeable Fe pools between biotic and abiotic systems,
485 which is explored in detail in the discussion.

486

487 **4. DISCUSSION**

488

489 In the following sections, we first focus on the extent of Fe reduction observed in
490 biotic and abiotic experiments conducted in low pH conditions, and then we compare the
491 rate and extent of DIR of ferrihydrite and goethite observed in this study to those
492 observed during previous experiments conducted at circumneutral pH. In this section, we
493 also evaluate the influence of substrate mineralogy and solution chemistry (e.g., pH,
494 dissolved PO_4^{3-}) on DIR activity. In addition, we discuss the extent of Fe(II)

incorporation into solids via sorption in low pH biotic and abiotic conditions. Finally, we explore the role of two possible mechanisms for the observed Fe isotope fractionation between $Fe(II)_{aq}$ and substrate Fe(III) in the current abiotic and DIR experiments at low pH: (1) ligand-promoted reductive dissolution and (2) Fe isotope exchange between $Fe(II)_{aq}$ and remaining solid Fe(III) to assess the potential of Fe isotopes as a biosignature in acidic systems.

4.1. Biotic and abiotic Fe reduction of ferric hydroxides at low pH

The significant amounts of Fe reduction by *Acidianus* strain DS80 for both ferrihydrite (~6%) and goethite (~11%) at pH ~3 over 19 days in this study are consistent with previous work on strain DS80 with either H_2 or S^0 as the electron donor (Amenabar et al., 2017; Amenabar and Boyd, 2018). In addition, strain DS80 can respire Fe(III) with numerous organic compounds as an electron donor (Amenabar et al., 2018). Previous experiments also showed that strain DS80 can couple DIR to growth without direct access to ferric hydroxides in acidic medium (Amenabar and Boyd, 2018). This implies that these cells could also facilitate the dissolution of Fe(III) hydroxides, possibly by releasing an extracellular chelator to increase the bioavailability of soluble Fe(III) (Amenabar and Boyd, 2018; Amenabar and Boyd, 2019). However, evidence in support of the production of such chelators has yet to be obtained experimentally. The very low Fe reduction (<1%) in the abiotic experiments are consistent with PHREEQC calculations considering the solution chemistry and the solubility of ferrihydrite and goethite at pH~3 (Ball and Nordstrom, 1991; Cornell and Schwertmann, 2003). These calculations suggest that the growth medium remained undersaturated with respect to ferrihydrite and goethite. It is possible that abiotic reductive dissolution of Fe(III) hydroxides by H_2 in the headspace of the reactor occurred, but to a limited extent due to its low solubility in aqueous medium at 80°C (Barrette and Sawyer, 1984; Choi, 2014). This reduction process, however, cannot explain results from biotic reactors, which showed a steady increase in $\%Fe(II)_{aq}$ over time accompanied with a concurrent increase in cell numbers (from ~$1.7 \cdot 10^5$ up to ~$1.6 \cdot 10^6$ cell/ml), as documented previously (Amenabar et al., 2017; Amenabar and Boyd, 2018). These observations indicate that cell growth was supported by coupled reduction of Fe(III) and oxidation of H_2 and DIR activity produced a larger quantity of $Fe(II)_{aq}$ compared to abiotic reactors.

Direct comparison of the extent of DIR between the current experiments at acidic pH and previous experiments at neutral pH is difficult, even for a particular substrate, due to different initial experimental conditions (cell density, solution chemistry, and duration). Hence, we compared the rate of Fe reduction normalized to $1.7 \cdot 10^5$ cell/ml as initial cell density, which is similar to our experimental condition (Table S.7; Supplementary Material). Previous experiments at neutral pH involving bacterial strains such as *Shewanella alga, Shewanella putrefaciens,* and *Geobacter sulfurreducens,*

observed lower rates of ~$3 \cdot 10^{-8}$ to ~$9 \cdot 10^{-8}$ %Fe reduction/min with low surface area goethite (SSA ≤55 m^2/g) compared to the rate of ~$4 \cdot 10^{-7}$ %Fe reduction/min with high surface area goethite (SSA ~153 m^2/g) (e.g., Roden and Zachara, 1996; Hansel et al., 2004; Crosby et al., 2005, 2007). In comparison, for goethite (SSA ~95 m^2/g) at acidic pH, we observed a faster rate of ~$4 \cdot 10^{-4}$ %Fe reduction/min by the archaeon *Acidianus* strain DS80. This observation suggests that the rate of DIR for goethite are not only function of available surface area and particle size as suggested previously (Roden and Zachara, 1996), but also could be influenced by the growth conditions such as solution pH and temperature. For instance, the higher solubility of goethite in acidic medium at 80°C could produce more bioavailable Fe(III) than that in a solution with pH ~7 at 25°C, resulting in a higher rate of DIR by thermoacidophiles.

For ferrihydrite, the comparison of Fe reduction rates observed here at acidic pH with previous DIR experiments conducted at neutral pH becomes more complex due to secondary mineral formation. At neutral pH, a wide range of Fe reduction rates of poorly crystalline ferrihydrite (~$3 \cdot 10^{-7}$ to $2 \cdot 10^{-2}$ % Fe reduction/min per $1.7 \cdot 10^5$ cell/ml as initial cell density) was documented in prior DIR experiments (Roden and Zachara, 1996; Fredrickson et al., 2003; Hansel et al., 2004; Amstaetter et al., 2012; Shimizu et al., 2013; Adhikari et al., 2017), most of which also reported transformation of ferrihydrite to secondary minerals (e.g., goethite, magnetite, siderite, green rust) upon interaction with microbially produced $Fe(II)_{aq}$. The rate of Fe reduction, $2 \cdot 10^{-4}$ % Fe reduction/min per $1.7 \cdot 10^5$ cell/ml density, observed in our cultures of DS80 at acidic pH, falls within this range, although no obvious mineralogical transformation was detected during19 days of incubation (Figure 5).

The ferrihydrite nanoparticles used in our study had higher surface area (~386 m^2/g) compared to the goethite nanocrystals (~95 m^2/g), which should lead to a higher % Fe reduction for ferrihydrite than goethite (Roden and Zachara, 1996). However, the extent of Fe(III) reduction in our cultures provided with nanocrystalline ferrihydrite (~6%) was less than those attained using nanocrystalline goethite (~11%) in acidic pH. This observation, however, contrasts with results from a previous experiments conducted with laboratory synthesized ferrihydrite and commercially available goethite particles, wherein it was hypothesized that a relationship exists between Fe(III) reduction rate, equilibrium solubility, and mineral crystallinity (Amenabar and Boyd, 2018). The surface area of the commercially available goethite was not determined in this previous study but it is possible (if not likely) that it is far lower than the synthetic nanoparticles used herein, potentially explaining the discrepancy.

Nonetheless, previous growth experiments with *Acidianus* strain DS80 showed that cells did not grow in close association with mineral particles (Amenabar et al., 2017). In growth conditions where ferrihydrite was sequestered in dialysis membranes, to inhibit physical contact with cells, strain DS80 could also grow via DIR (Amenabar and Boyd, 2018). These observations suggest that *Acidianus* cells reduce soluble Fe(III) produced

by dissolution of the solid substrates, rather than relying solely on directly reducing solid Fe(III) substrates. This observation rules out the possibility of a preference for specific substrate such as ferrihydrite or goethite during DIR by strain DS80.

The subtle difference in % Fe reduction between the two minerals could possibly be attributed to the small variations in the reactor-specific conditions (e.g., initial mass of solid Fe(III) and initial cell density). Another possibility would be different available reactive sites on goethite and ferrihydrite surfaces that might influence solubility. Differences in the extent of aggregation between ferrihydrite and goethite at pH~3 may impact their effective solubility/availability and thus the extent of DIR under acidic conditions used to cultivate strain DS80. Ferrihydrite nanoparticles are observed to aggregate noticeably even at pH < 4 (Yuwono et al., 2012), and this may reduce the available reactive surface area, and thereby effectively decreasing its solubility. In contrast, goethite nanocrystals show less aggregation at acidic pH (Cwiertny et al., 2008), indicating that a higher effective surface area may be available for solubilization of goethite compared to ferrihydrite in our experiments. We speculate that less aggregation of goethite compared to ferrihydrite at low pH may have caused a greater extent of DIR of goethite compared to ferrihydrite.

Dissolved anions such as PO_4^{3-}, SO_4^{2-}, Cl^- that sorb onto ferric hydroxides, could also contribute to the suppressed reducibility of ferrihydrite compared to goethite (e.g., Geelhoed et al., 1997; Liu et al., 1999; Mallet et al., 2013; Zhu et al., 2014; Gu et al., 2016; Schulthess and Ndu, 2017; Essington and Stewart, 2018). However, in a complex medium, like ours, with multiple competing anions, the sorption affinity of PO_4^{3-} onto a ferric hydroxide is stronger than other anions (Geelhoed et al., 1997; Mallet et al., 2013; Essington and Stewart, 2018). Hence, we focus on the effect of PO_4^{3-} on these ferric hydroxides as our growth medium has ~2.4 mM PO_4^{3-}. Sorption of PO_4^{3-} on Fe(III) hydroxides is known to influence their accessibility to microbes (Zachara et al., 1998; Celi et al., 2000; Borch et al., 2007; Borch and Fendorf, 2008; Amstaetter et al., 2012). Ferrihydrite nanoparticulates can sorb more PO_4^{3-} from solution than goethite and the extent of PO_4^{3-} sorption onto ferrihydrite and goethite tends to increase at lower pH (Zachara et al., 1998; Celi et al., 2000). Surface coverage by PO_4^{3-} decreases the availability of surface Fe(III) atoms of ferrihydrite to microbial reductive dissolution to a greater extent than in goethite (Zachara et al., 1998; Borch et al., 2007; Borch and Fendorf, 2008; Amstaetter et al., 2012). Although we have not monitored PO_4^{3-} concentration in the solution over the experimental duration, it is likely that PO_4^{3-} was sorbed onto ferric-hydroxide surfaces similar to previous experiments with comparable dissolved PO_4^{3-} concentration (Zachara et al., 1998; Celi et al., 2000). Such processes could mask the actual reducibility of ferrihydrite and could result in a slightly lesser solubility and/or extent of reductive dissolution of ferrihydrite compared to goethite. Validating these hypotheses will require further experimentations dedicated to deconvoluting the specific influences of each of these variables.

4.2. Incorporation of Fe(II) into solid substrates during Fe reduction at low pH

The proportion of solid-phase Fe(II) in the biotic reactors decreased exponentially with time from relatively high values (~6% in ferrihydrite and ~14% in goethite) at day 2 to <1% at day 19 for both minerals (Figure S.3). In contrast, very little incorporation of Fe(II) into ferric hydroxides (2-3% in ferrihydrite and 3-5% in goethite) occurred in abiotic reactors with no obvious temporal trends (Figure S.3). Overall, the low extent of Fe(II) incorporation into solids at the end of the experiments is consistent with the limited extent of Fe(II) sorption on Fe-hydroxides (~3-11%; Figure S.4) as expected from previous abiotic experiments conducted at pH ~2.5 (Reddy et al., 2015).

Incorporation of solid-phase Fe(II) early in the biotic reactors might have occurred via transfer of electrons from solution to ferric (hydr)oxide surfaces followed by transportation to the interior of the solids via an "e^- hopping" mechanism (Rosso et al., 2003; Iordanova et al., 2005; Katz et al., 2012; Alexandrov and Rosso, 2014). Early precipitation of mixed-valence Fe minerals (e.g., green rust, magnetite) on ferric (hydr)oxide surfaces could also introduce Fe(II) into the solids. The estimated fractionation between $Fe_{extracted}$ and $Fe(II)_{aq}$ (i.e., $\Delta^{56}Fe_{Fe_{extracted}-Fe(II)_{aq}}$) ranges between ~ 2.3 to 3.0‰ (ferrihydrite) and ~ 1.2 to 1.9‰ (goethite) (Table 5). These values are quite different from the -0.25‰ equilibrium fractionation reported between green rust and $Fe(II)_{aq}$ at room temperature (Wiesli et al., 2004) suggesting that the Fe(II) in the HCl-extracted Fe in our experiments was not from the dissolution of mixed-valence green rust. The equilibrium $^{56}Fe/^{54}Fe$ fractionation between magnetite and $Fe(II)_{aq}$ at room temperature (~1.30 to 1.56‰; Johnson et al., 2005; Frierdich et al., 2014b), on the other hand, falls close to the estimated range of $\Delta^{56}Fe_{Fe_{extracted}-Fe(II)_{aq}}$, particularly for goethite. The nature of early solid-phase Fe(II) incorporation during biological reduction is unclear, but the absence of any detectable secondary minerals including magnetite, as confirmed by XRD analysis and FE-SEM images of post-incubation solids eliminates magnetite or any other new Fe(II)-bearing minerals as the probable source of Fe(II) in HCl-extracted Fe.

4.3. Mechanisms of Fe isotope fractionation during Fe reduction at low pH

In this section we evaluate two mechanisms for producing the measured Fe isotope fractionations: 1) ligand-promoted isotopic effects and 2) equilibrium Fe isotope exchange between reactive Fe(III) and Fe(II) pools. Early experiments on Fe isotope fractionation have documented a role for organic ligands, and Wiederhold et al. (2006) documented $^{56}Fe/^{54}Fe$ fractionations for goethite of similar magnitude (~1.1‰) to what we measured, in the early stages of their experiments in both abiotic ligand-promoted (in the dark) and reductive dissolution (in the light) of goethite by oxalate at pH ~3. In their

study, oxalate facilitated the dissolution of goethite via production of a $Fe(III)_{aq}$-oxalate complex, which in the presence of light was photochemically reduced to $Fe(II)_{aq}$. Similarly, we observed an increase in $\delta^{56}Fe_{aq,\,tot}$ values towards the bulk solid values (~ 0‰) over time in our biotic reactors for both minerals. In the early stage of the experiments by Wiederhold et al. (2006), the strong isotopic fractionation between dissolved Fe and Fe(III) in the bulk solid was interpreted as a kinetic isotope effect, where preferential dissolution of lighter Fe isotopes during rapid oxalate-promoted dissolution produced surface sites enriched in heavier isotopes. With progressive dissolution, the solid surfaces enriched with heavier isotopes started to dissolve and the isotopic contrast between the solid and fluid Fe decreased over time. In the late stage of both oxalate-promoted goethite dissolution in the dark (>7 days) and reduction in the light (>3 hours) the $\delta^{56}Fe_{aq}$ values became slightly positive and, over longer duration, these values remained unchanged. This observation was interpreted as an equilibrium isotope effect where dissolved Fe-ligand complexes became enriched in heavier isotopes relative to the bulk goethite.

Given that *Acidianus* cells can reduce ferric (hydr)oxides in acidic medium, even without direct contact (Amenabar and Boyd, 2018), it is possible that cells produce an organic ligand(s), which may facilitate dissolution of Fe(III), allowing for it to serve as a substrate for DIR. Comparison between the temporal trends in $^{56}Fe/^{54}Fe$ fractionation between Fe(III) in bulk goethite and $Fe_{aq,\,tot}$ in our biotic experiments (Table S.8; Supplementary Material) and the data reported in Wiederhold et al. (2006) suggests that, during ligand-promoted dissolution and reduction, the bulk goethite was not in isotopic equilibrium with the dissolved fraction (Figure 8A). Likewise, in our experiments, the $^{56}Fe/^{54}Fe$ fractionation between Fe(III) in bulk ferrihydrite and $Fe_{aq,\,tot}$ also decreased with time, although by a smaller magnitude (~2.8‰ to ~2.4‰) compared to that in goethite (~1.1‰ to ~0.17‰), which might be interpreted to record a kinetic effect as proposed by Wiederhold et al. (2006). However, unlike the observation by Wiederhold et al. (2006), during 19 days, the $\delta^{56}Fe_{aq,\,tot}$ values never became higher than the initial bulk solid values in our study. Therefore, although the kinetic ligand-promoted reductive dissolution model proposed by Wiederhold et al. (2006) can explain the data from the early stage of our biotic experiments, their late stage equilibrium fractionation model between ligand-bound Fe(II) and solid Fe(III) does not explain our experimental data in the final stages; one possible explanation for this is that isotopic equilibrium was never attained in our experiments between bulk solid and $Fe(II)_{aq}$. Instead a relatively smaller temporal variability in the $\Delta^{56}Fe_{Fe(III)_{reac}-Fe(II)_{aq}}$ from biotic reactors (goethite: 1.57±0.52‰ and ferrihydrite: 2.91±0.40‰) implies that the $Fe(II)_{aq}$ and surface-bound reactive Fe(III) may have achieved a near-equilibrium condition (Figure 8B).

One approach for considering the isotopic effects of ligand-bound Fe(III) is to consider the β-values (expressed as $1000 \cdot \ln(\beta)$) for the $^{56}Fe/^{54}Fe$ previously calculated for ligand-bound Fe(III) using the Density Function Theory (Domagal-Goldman and

692 Kubicki, 2008). If ligand-promoted dissolution is the sole mechanism in our biotic
693 experiments, and the main species involved in $^{56}Fe/^{54}Fe$ fractionation are solid surface-
694 bound Fe(III)-oxalate complexes and $[Fe(II)(H_2O)_6)]^{2+}$ in solution, we obtain an
695 equilibrium $\Delta^{56}Fe_{Fe(III)\text{-}oxalate\text{-}[Fe(II)(H2O)6]2+}$ of 1.68‰ (In vacuo model) and 1.41‰
696 (Integrated Equation Formalism Polarized Continuum Model or IEFPCM) using β-values
697 at 80°C (Domagal-Goldman and Kubicki, 2008; Table S.9). The calculated
698 $\Delta^{56}Fe_{Fe(III)_{reac}-Fe(II)_{aq}}$ values in our study show wider ranges (goethite: 1.20‰ to
699 1.98‰ and ferrihydrite: 2.53‰ to 3.23‰; Table 5) than those predicted Fe isotope
700 fractionation between Fe(III)-oxalate and $Fe(II)_{aq}$. Note that this approach does not
701 consider aqueous ligand-bound Fe(III), as $Fe(III)_{aq}$ contents in our experiments were very
702 low, with the exception of the last time points (discussed below). Although the isotopic
703 fractionation between solid-bound Fe(III)-oxalate and aqueous $[Fe(II)(H_2O)_6)]^{2+}$ overlaps
704 those in our goethite experiments, these predicted fractionation values plot far from the
705 results for the ferrihydrite experiments (Figure 6), and it seems special pleading for a
706 ligand effect only in the goethite experiments but not in the ferrihydrite experiments.
707 Such observations weigh against explaining all of the Fe isotope variations by a ligand
708 model, despite the fact that the addition of organic acids to goethite suspensions may
709 increase the size of surface-bound labile Fe(III) pool that participates in Fe isotope
710 exchange (Reichard et al., 2007).

711 Rigorous testing of a ligand-promoted reductive dissolution model is difficult, as
712 there is no direct evidence that *Acidianus* cells produce an organic ligand (e.g., oxalate)
713 during DIR. Importantly, previous experiments with *Acidianus* showed that both cell
714 growth and Fe(III) reduction activity were enhanced by ~2-fold when direct access to
715 solid Fe(III)-hydroxide surfaces was permitted, in contrast to the condition where
716 minerals were sequestered in dialysis membranes with molecular-weight cutoffs of 6-8
717 kDa and 12-14 kDa to prevent direct access (Amenabar and Boyd, 2018). In fact, similar
718 rates of cell growth and Fe(III) reduction were observed in experiments where Fe(III)
719 hydroxides were contained in membranes with 6-8 kDa or 12-14 kDa, indicating that any
720 organic compound promoting Fe dissolution/reduction must be, on average, <60 amino
721 acids or smaller if protein or <6 kDa if non-protein. Additional difficulty arises in the
722 very high levels of ligands used in the experiments by Wiederhold et al. (2006), which
723 were conducted in the presence of ~1 mM oxalate; this is an order of magnitude higher
724 than the usual concentration range of dissolved oxalate found in nature (few μM to
725 several hundred μM; Jones, 1998; Jones et al., 2003; Adeleke et al., 2017). Therefore,
726 despite the possibility that *Acidianus* cells produced organic acids, it is unlikely that the
727 concentration of that organic acid would exceed a few hundred μM.

728 Alternatively, we prefer to interpret the isotopic fractionations between $Fe(II)_{aq}$
729 and solid Fe(III) to reflect Fe isotope exchange during electron transfer, following the
730 models of Crosby et al. (2005, 2007) that were developed from experiments at neutral
731 pH. This model provides the best explanation for the contrast in Fe isotope fractionations

between the two substrates (goethite and ferrihydrite), which is difficult to reconcile with a ligand model. Although sorbed Fe(II) is expected to be low in our acidic conditions (Handler et al., 2014; Reddy et al., 2015), if isotopic exchange at mineral-fluid interface is rapid relative to the detachment rate of Fe(II) produced during reduction, isotopic exchange would still occur. The substantial increases in both $Fe(II)_{aq}$ concentration and $\delta^{56}Fe_{aq,\,tot}$ values (by ~0.5‰ for ferrihydrite and ~0.9‰ for goethite) towards the $\delta^{56}Fe$ value of initial solids during DIR is entirely consistent with such coupled electron transfer and isotope exchange mechanisms involving sizeable reactive Fe pools (i.e., $Fe(II)_{aq}$ and substrate). In contrast, small temporal changes in $Fe(II)_{aq}$ concentration and $\delta^{56}Fe_{aq,\,tot}$ values in abiotic reactors for both minerals, imply that a limited extent of abiotic dissolution and reduction of Fe(III) hydroxide was accompanied by a small Fe isotope exchange involving small pools of reactive Fe.

Several extracellular electron transfer mechanisms (e.g., *c*-type cytochromes, soluble electron shuttles, and electrically conductive pili or nanowires) have been reported for Fe-reducing microbes at neutral pH (Reguera et al., 2005; Lovley, 2012; Holmes et al., 2016; Shi et al., 2016). The presence of hair-like appendages resembling "nanowires" were observed extending from the surface of *Acidianus* strain DS80 cells when grown with solid ferric (hydr)oxides but not when cells were grown with other electron acceptors such as S^0 (Amenabar et al., 2017). However, the conductive properties of these nanowires or their involvement in DIR have yet to be firmly established. Hence, we may only speculate that, in the absence of sorbed Fe(II) at low pH, the reductive dissolution and associated electron and isotope exchange at mineral-fluid interface might have been facilitated by these extracellular appendages.

Assuming the Fe isotope fractionations between $Fe(III)_{reac}$ and $Fe(II)_{aq}$ reflects equilibrium isotopic partitioning, the equilibrium goethite-$Fe(II)_{aq}$ fractionation at 80°C is expected to be ~0.73‰ (Beard et al., 2010), and yet our experiments show significantly higher $\Delta^{56}Fe_{Fe(III)_{reac}-Fe(II)_{aq}}$ values (abiotic: 1.98±0.49‰, biotic: 1.57±0.52‰; Figure 6B). One explanation is that the surface Fe(III) atoms are bonded differently after undergoing electron and atom exchange, reflecting a distorted lattice, compared to the atoms in the underlying bulk mineral. Crosby et al. (2005, 2007) proposed this as an explanation for the relatively large $Fe(III)_{reac}$-$Fe(II)_{aq}$ Fe isotope fractionations in their DIR experiments with micro-goethite at neutral pH, which if extrapolated to 80°C, were ~1.87‰ that overlaps those measured in our study. Similarly, high fractionation values estimated between Fe(III) on the nano-goethite surface and $Fe(II)_{aq}$ (~1.47‰, extrapolated to 80°C) in abiotic experiments by Beard et al. (2010) agrees with our observation. In comparison, $\Delta^{56}Fe_{Fe(III)_{reac}-Fe(II)_{aq}}$ values in our ferrihydrite experiments (abiotic: 2.79±0.37‰ and biotic: 2.91±0.40‰; Figure 6A) are close to the equilibrium ferrihydrite-$Fe(II)_{aq}$ fractionation (~2.28‰, extrapolated to 80°C; Wu et al., 2011) implying a less pronounced structural difference between $Fe(III)_{reac}$ and bulk

771 ferrihydrite compared to that observed for goethite. This could suggest that a ferrihydrite-
772 like distorted structure may broadly represent $Fe(III)_{reac}$ regardless of the initial substrate.
773 With progressive DIR, significant increase in the proportion of the distorted
774 $Fe(III)_{reac}$ (i.e., $X_{Fe(III)_{reac}}$ ≤0.62 and 0.19 for ferrihydrite and goethite, respectively; Fig.
775 7), might explain the rise in $Fe(III)_{aq}$ at the end of the biotic experiments. We speculate
776 that the high $Fe(III)_{aq}$ content reflects an increase in the solubility of the substrates upon
777 reaction with $Fe(II)_{aq}$ during microbial reduction. Previous Mössbauer studies have
778 documented that upon interaction with dissolved Fe(II), surface Fe(III) sites become
779 more distorted or defect-rich relative to the underlying unreacted Fe(III) (e.g., Williams
780 and Scherer, 2004). This observation is also consistent with recent spectroscopic studies
781 (e.g., Notini et al., 2018, 2019) and a study using atom probe tomography with ^{57}Fe
782 isotope as a tracer (Taylor et al., 2019) that demonstrated the important role of defects on
783 goethite surface in facilitating electron transfer and isotope exchange between $Fe(II)_{aq}$
784 and surface Fe(III). If the distorted surface Fe(III) are more soluble than the underlying
785 bulk mineral, it could potentially enhance the overall solubility of the minerals at pH ~3.
786 Alternatively, the $Fe(III)_{aq}$ may be complexed by organic ligands that were not present in
787 the early stage of DIR. If the growth rate and DIR activity declined at day 19 it is
788 possible for the ligand-bound Fe(III) to be more detectable. However, we did not observe
789 any decline in cell growth or DIR activity over 19 days in any experiments with
790 *Acidianus* (e.g., Amenabar et al., 2017; Amenabar and Boyd, 2018; this study).
791 Therefore, it is unlikely that the excess $Fe(III)_{aq}$ observed at day 19 are the result of
792 ligand production.
793 We summarize our model in Figure 9, which is a modification of the conceptual
794 model developed for neutral-pH conditions by Crosby et al. (2005, 2007), and adapted to
795 the low-pH conditions of the current work:
796
797 Stage 1:

798 • Abiotic (proton-promoted) and biotic (proton-promoted and/or ligand-controlled
799 if produced by *Acidianus*) dissolution to produce $Fe(III)_{aq}$ on ferric hydroxide
800 surfaces (reaction a, Figure 9).

801 • Immediately after formation, reduction of $Fe(III)_{aq}$ ions to $Fe(II)_{aq}$ at the mineral-
802 fluid interface either directly by dissolved H_2 (abiotic) or catalyzed by *Acidianus*
803 strain DS80 cells (biotic) (reactions b and c, Figure 9).

804 Stage 2:

805 • At the mineral-fluid interface, newly formed $Fe(II)_{aq}$ ions instantaneously
806 participate in electron transfer and isotope exchange with $Fe(III)_{reac}$ on the surface
807 of ferric hydroxides leading to the $\Delta^{56}Fe_{Fe(III)_{reac}-Fe(II)_{aq}}$ of ~1.6-2.9‰ (reaction
808 d, Figure 9).

Stage 3:

- At low pH, the sorption of Fe(II) on the mineral surface is unfavorable, leading to the release of virtually all Fe(II) into solution (reaction e, Figure 9).
- Electron transfer and Fe isotope exchange at the mineral-fluid interface produces structurally distorted reactive Fe(III) on the mineral surface with δ^{56}Fe values that are higher (goethite) or similar (ferrihydrite) to the initial substrate.
- For biotic reactors, when the fraction of $Fe(III)_{reac}$ becomes considerably large (~20% for goethite and ~60% for ferrihydrite), $Fe(III)_{aq}$ is detected, reflecting the increased surface solubility (reaction f, Figure 9).

Our model suggests that positive feedbacks may occur between microbial activity and enhanced substrate availability during DIR at acidic pH. Such geobiological feedbacks between microbial activity and their habitats are expected to increase the competitive advantage of DIR thermoacidophiles and are likely to positively influence the fitness of their progeny via "niche construction" (Odling-Smee et al., 1996; Colman et al., 2018). Although the biogeochemical impact of such a phenomenon in this strain is still unexplored in regards to Fe cycling, the role of such feedbacks on DS80 has been studied when grown under S^0 reducing and disproportionating conditions (Amenabar and Boyd, 2018; 2019). Based on our results, we propose that direct or indirect modification of mineral substrates catalyzed by the DIR activity of *Acidianus* strain DS80 took place. If a similar process occurs in acidic hot springs, this phenomenon could lead to an advantage for cells competing for electron donors or carbon sources.

4.4. Are Fe isotopes a biosignature for DIR at low pH?

The extent of Fe isotope exchange between dissolved Fe(II) and Fe(III)-hydroxides may serve as a measure for the reactivity of iron minerals and the magnitude of Fe cycling via abiotic and biotic processes under certain environmental conditions. In this section, we compare the relative proportion of the reactive Fe(III) pool, defined here as "$\%Fe(III)_{reac}$" (i.e., $X_{Fe(III)_{reac}}$ expressed in %; Eq. 7), which is equivalent to the "%Fe exchanged" used in Fe isotope tracer studies (e.g., ^{55}Fe, ^{57}Fe, ^{59}Fe), across various pH conditions to illustrate the significance of microbial activity in Fe cycling at acidic pH.

The % Fe exchange between $Fe(II)_{aq}$ and goethite shows a distinct increase as a function of solution pH under abiotic conditions (Figure 10), consistent with a model where the extent of exchange depends on the quantity of sorbed Fe(II) (Frierdich et al., 2014a; Handler et al., 2014; Reddy et al., 2015). At pH >6, a wide variability in the extent of Fe isotope exchange (~20-90%, Figure 10) has been reported in abiotic experiments between goethite and $Fe(II)_{aq}$ (Handler et al., 2014; Frierdich et al., 2014a; Reddy et al., 2015; Joshi et al., 2017), where the range reflects varying experimental conditions, including surface area and $Fe(II)_{aq}$ contents. Two biotic (DIR) experiments with goethite at pH >6 are available, which show a maximum of ~5% $Fe(III)_{reac}$ (Crosby

et al., 2005, 2007). It is challenging to compare these values directly to the abiotic experiments at circumneutral pH, as the extent of DIR is a complex function of substrate composition, growth medium, and cell density. More importantly, during DIR small quantities Fe(II) is continuously produced *in situ* over time, which is entirely different from the approach used in the abiotic experiments, where a large quantity of $Fe(II)_{aq}$ is added at the start of an experiment. We would therefore broadly expect that for the same substrate and pH, the $\%Fe(III)_{reac}$ for biotic DIR experiments will be less than those of "equivalent" abiotic experiments, recognizing that the $Fe(II)_{aq}$-time relations are quite different.

The low $\%\ Fe(III)_{reac}$ (~2%) estimated from the abiotic experiments in this study using goethite at pH ~3 is in good agreement with previous abiotic experiments at low pH using an ^{57}Fe tracer approach (Reddy et al., 2015). However, the $\%\ Fe(III)_{reac}$ values calculated from our biotic experiments at pH ~3 are an order of magnitude greater (~20%) than that in abiotic experiments carried out at similar pH (Figure 10). This contrast is opposite to the expected outcomes, as noted above, where abiotic experiments should produce a greater extent of Fe isotope exchange than biotic experiments. This observation indicates a clear role of DIR at low-pH in catalyzing Fe isotope exchange that would otherwise be inhibited at low pH due to the lack of sorbed Fe(II). This role of biology is quite different than that proposed for Fe isotope exchange at circumneutral pH, where DIR only serves as a source of $Fe(II)_{aq}$, rather than a direct "vital effect" that catalyzes Fe isotope exchange (Crosby et al., 2005, 2007; Wu et al., 2010). Importantly, this contrast in biotic and abiotic systems holds regardless of the mechanism of isotopic exchange (ligand-controlled versus electron transfer/atom exchange).

At circumneutral pH, pure ferrihydrite is susceptible to rapid transformation to more stable phases, making experiments aimed at characterizing $Fe(III)_{reac}$ difficult (Hansel et al., 2003; Jang et al., 2003; Hansel et al., 2005; Johnson et al. 2005; Pedersen et al., 2005; Boland et al., 2014). Therefore, the results from only a few abiotic experiments with ferrihydrite at pH >6 that showed minimal mineralogical changes (Jones et al., 2009) are comparable to our simple $Fe(II)_{aq}$-ferrihydrite experiments. These previous studies reported a wide range of Fe isotope exchange varying from ~44% (freeze-dried ferrihydrite) to 65-100% (undried ferrihydrite with 25-150 ppm dissolved organic matter). The extent of Fe exchange in experiments involving poorly-crystalline ferrihydrite at pH <6, however, is not well documented because of the high solubility of ferrihydrite in acidic solutions (e.g., Fox, 1988). Our abiotic experiments at pH ~3 document a very limited extent of Fe isotope exchange ($\%\ Fe(III)_{reac} \leq 9\%$) in ferrihydrite, in contrast to a significantly high extent of Fe isotope exchange (≤60%) observed in our DIR experiments. As with the results using goethite, these observations point towards a clear catalytic role of biology in promoting Fe isotope exchange under acidic conditions.

Significant production of low-$\delta^{56}Fe$ $Fe(II)_{aq}$ by DIR in acidic systems should be detectable in many acidic environments. Nanoparticulate ferric hydroxides, such as

888 goethite and ferrihydrite, as well as soluble $Fe(III)_{aq}$, are abundant in a wide range of
889 natural environments including extreme acidic and anoxic conditions (e.g., acidic
890 hydrothermal springs, acid mine drainages, acidic riverine systems such as Rio Tinto
891 River Basin; Jambor and Dutrizac, 1998; Langner et al., 2001; Hassellöv and von der
892 Kammer, 2008; Amenabar and Boyd, 2018; 2019). Abiotic oxidation of $Fe(II)_{aq}$ in acidic
893 conditions is an unlikely mechanism for producing low-δ^{56}Fe $Fe(II)_{aq}$ because of strong
894 kinetic inhibitions even under high-O_2 conditions (Millero, 1985; Stumm and Morgan
895 1996; Morgan and Lahav, 2007). Importantly, the significant extent of isotopic exchange
896 catalyzed by DIR should produce high-δ^{56}Fe ferric hydroxides. In addition, the lack of
897 substantial Fe(II) sorption at low-pH indicates that the DIR-generated low-δ^{56}Fe Fe(II)
898 component will not reside in the solids, but instead should remain as $Fe(II)_{aq}$. This
899 contrasts with DIR at circumneutral pH, where the majority of Fe(II) resides in the solid
900 phase, as demonstrated in experiments and natural systems (e.g., Canfield et al., 1993),
901 which significantly affects Fe isotope mass balance (Percak-Dennett et al., 2013). The
902 applicability of Fe isotopes to search for microbial activity in low-pH environments could
903 also be extended to non-Earth systems, such as extraterrestrial acidic systems (e.g.,
904 Martian paleoenvironments) where ferric (hydr)oxides were possibly abundant
905 (Fernández-Remolar et al., 2005; Bibring et al., 2006; Morris et al., 2006; Hurowitz and
906 McLennan, 2007; Morris et al., 2008; Hurowitz et al., 2010; Dauphas et al., 2012;
907 Peretazkho et al., 2018) to support mineral-based microbial metabolism (Boston et al.,
908 1992; Horneck, 2000; Cabrol et al., 2001; Nixon et al., 2013).
909
910 **5. CONCLUSIONS**
911
912 In acidic anoxic conditions, DIR of ferrihydrite and goethite by *Acidianus* strain
913 DS80 produces substantial Fe isotope fractionation and exchange between DIR-produced
914 $Fe(II)_{aq}$ and ferric hydroxides. Such an observation was unexpected based on prior work
915 in abiotic systems that showed limited Fe isotope exchange at low pH because of the
916 absence of significant sorbed Fe(II). Regardless of the Fe(III) mineral substrate provided,
917 $Fe(II)_{aq}$ produced by DIR in the low-pH experiments always had low δ^{56}Fe values,
918 reflecting isotopic mass balance to the high δ^{56}Fe values of the outermost reactive Fe(III)
919 extracted from solids. Either ligand-promoted dissolution or coupled electron transfer and
920 isotope exchange between the $Fe(II)_{aq}$ and $Fe(III)_{reac}$ during DIR could produce such Fe
921 isotope fractionation at acidic pH. However, due to a lack of experimental data indicating
922 whether *Acidianus* cells produce any organic ligands, it is more likely that coupled
923 electron transfer and isotope exchange was primarily responsible for our observed Fe
924 isotope fractionation, compared to ligand-controlled dissolution. This conclusion is
925 supported by the substrate-dependent Fe isotope fractionations between $Fe(III)_{reac}$ and
926 $Fe(II)_{aq}$ that would not be observed if the Fe(III) component was entirely ligand-bound
927 Fe(III).

The extent of Fe(II) sorption in both abiotic and biotic reactors was insignificant at pH ~3. However, considering Fe isotope exchange between solid Fe(III) and $Fe(II)_{aq}$, we find a temporal increase in the fraction of $Fe(III)_{reac}$ ($X_{Fe(III)_{reac}}$) during DIR of both ferrihydrite and goethite. In contrast, the $X_{Fe(III)_{reac}}$ was negligible in abiotic reactors for both minerals. Because all experiments were performed at acidic pH, where the role of Fe(II) sorption is expected to be trivial, we can conclude that electron transfer and atom exchange is mainly catalyzed by DIR. The $\Delta^{56}Fe_{Fe(III)_{reac}-Fe(II)_{aq}}$ values for goethite in biotic reactors (1.57±0.52‰) is higher than the equilibrium goethite-$Fe(II)_{aq}$ fractionation factor (~0.73‰ at 80°C; Beard et al., 2010), suggesting that the surface reactive layer produced during Fe isotope exchange between $Fe(II)_{aq}$ and goethite in biotic reactors had a different structure. This reactive Fe(III) layer may be defect-rich, more soluble, and more distorted compared to the starting goethite, similar to that inferred to be produced by DIR of goethite under circumneutral pH (Crosby et al., 2005, 2007). In comparison, the $\Delta^{56}Fe_{Fe(III)_{reac}-Fe(II)_{aq}}$ values for ferrihydrite in biotic reactors (2.91±0.40‰) were relatively closer to the equilibrium ferrihydrite-$Fe(II)_{aq}$ fractionation factor (~2.28‰ at 80°C; Wu et al., 2011), implying some structural similarity between the bulk ferrihydrite and the reactive Fe(III) on ferrihydrite surface. In this sense, the altered reactive surface layer in the goethite may share similar characteristics with poorly crystalline ferrihydrite. The production of such a distorted and more soluble reactive surface layer on the mineral substrate during DIR also suggests a positive geobiological feedback process, where DIR-produced $Fe(II)_{aq}$ modifies the residual substrates via electron transfer and isotope exchange, which, in turn, increases the bioavailability of Fe(III) and thereby may enhance the fitness or selectivity of the modifying organism and their progeny.

Regardless of the mechanisms involved in Fe isotope fractionation in this study (i.e., either ligand-promoted dissolution or DIR-induced electron/atom exchange), the outcomes of the current experiments clearly demonstrate that the biotic experiments produced a much larger pool of exchangeable Fe than the abiotic experiments. Based on these observations, we conclude that at low pH, thermoacidophiles (e.g., *Acidianus* spp.) are capable of promoting extensive Fe cycling via DIR coupled with Fe isotope exchange between ferric hydroxides and $Fe(II)_{aq}$, which is, otherwise, very limited in low pH abiotic systems. Therefore, these results indicate the possibility of a significant isotopic fractionation among Fe components in acidic anoxic systems if thermoacidophilic DIR microbes are present and active. This highlights the potential application of Fe isotopes as biosignatures in ancient and modern anaerobic terrestrial and extraterrestrial acidic environments.

6. ACKNOWLEGEMENTS

This research was supported by a grant from the NASA Astrobiology Institute (NNA13AA94A). The authors gratefully acknowledge use of facilities and

instrumentation at the UW-Madison Wisconsin Centers for Nanoscale Technology (wcnt.wisc.edu) partially supported by the NSF through the University of Wisconsin Materials Research Science and Engineering Center (DMR-1720415). The authors are thankful to Susann Henkel and two other anonymous external reviewers and the associate editor Hailiang Dong for their time and constructive comments.

7. APPENDIX A. SUPPLEMENTARY MATERIAL

Additional methods, data tables, and figures are provided in the Supplementary Material.

REFERENCES

Adeleke R., Nwangburuka C. and Oboirien B. (2017) Origins, roles and fate of organic acids in soils: A review. *S. Afr. J. Bot.* **108**, 393–406.

Adhikari D., Zhao Q., Das K., Mejia J., Huang R., Wang X., Poulson S. R., Tang Y., Roden E. E. and Yang Y. (2017) Dynamics of ferrihydrite-bound organic carbon during microbial Fe reduction. *Geochim. Cosmochim. Acta* **212**, 221–233.

Alexandrov V. and Rosso K. M. (2014) Electron transport in pure and substituted iron oxyhydroxides by small-polaron migration. *J. Chem. Phys.* **140**, 234701

Amenabar M. J. and Boyd E. S. (2019) A review of the mechanisms of mineral-based metabolism in early Earth analog rock-hosted hydrothermal ecosystems. *World J. Microbiol. Biotechnol.* **35**, 29. Available at: http://link.springer.com/10.1007/s11274-019-2604-2.

Amenabar M. J. and Boyd E. S. (2018) Mechanisms of mineral substrate acquisition in a thermoacidophile. *Appl. Environ. Microbiol.* **84**, 1–18. Available at: http://aem.asm.org/lookup/doi/10.1128/AEM.02264-10.

Amenabar M. J., Colman D. R., Poudel S., Roden E. E. and Boyd E. S. (2018) Electron acceptor availability alters carbon and energy metabolism in a thermoacidophile. *Environ. Microbiol.* **20**, 2523–2537.

Amenabar M. J., Shock E. L., Roden E. E., Peters J. W. and Boyd E. S. (2017) Microbial substrate preference dictated by energy demand rather than supply. *Nat. Geosci.* **10**, 577–581.

Amstaetter K., Borch T. and Kappler A. (2012) Influence of humic acid imposed changes of ferrihydrite aggregation on microbial Fe (III) reduction. *Geochim. Cosmochim. Acta* **85**, 326-341.

Atlas R. M. (1997) *Handbook of microbiological media.* CRC Press, New York, NY.

Ball J. W. and Nordstrom D. K. (1991) User's manual for WATEQ4F, with revised thermodynamic data base and test cases for calculating speciation of major, trace, and redox elements in natural waters. *U.S. Geol. Surv. Water-Resources Investig. Rep.* **91–183**. Available at: http://wwwbrr.cr.usgs.gov/projects/GWC_chemtherm/pubs/wq4fdoc.pdf.

Barrette W. C. and Sawyer D. T. (1984) Determination of dissolved hydrogen and effects of media and electrode materials on the electrochemical oxidation of molecular hydrogen. *Anal. Chem.* **56**, 653–657.

1010 Beard B. L., Handler R. M., Scherer M. M., Wu L., Czaja A. D., Heimann A. and
1011 Johnson C. M. (2010) Iron isotope fractionation between aqueous ferrous iron and
1012 goethite. *Earth Planet. Sci. Lett.* **295**, 241–250. Available at:
1013 http://dx.doi.org/10.1016/j.epsl.2010.04.006.
1014 Beard B. L., Johnson C. M., Cox L., Sun H., Nealson K. H. and Aguilar C. (1999) Iron
1015 isotope biosignatures. *Science* **285**, 1889–1892.
1016 Beard B. L., Johnson C. M., Skulan J. L., Nealson K. H., Cox L. and Sun H. (2003)
1017 Application of Fe isotopes to tracing the geochemical and biological cycling of Fe.
1018 *Chem. Geol.* **195**, 87–117.
1019 Bibring J., Langevin Y., Mustard J. F. and Arvidson R. (2006) Global Mineralogical and
1020 Aqueous Mars History Derived from OMEGA/Mars Express Data. *Science* **312**,
1021 400–405.
1022 Boland D. D., Collins R. N., Miller C. J., Glover C. J. and Waite T. D. (2014) Effect of
1023 solution and solid-phase conditions on the Fe(II)-accelerated transformation of
1024 ferrihydrite to lepidocrocite and goethite. *Environ. Sci. Technol.* **48**, 5477–5485.
1025 Borch T., Masue Y., Kukkadapu R. K. and Fendorf S. (2007) Phosphate imposed
1026 limitations on biological reduction and alteration of ferrihydrite. *Environ. Sci.*
1027 *Technol.* **41**, 166–172.
1028 Borch T. and Fendorf S. (2008) Phosphate Interactions with Iron (Hydr)oxides:
1029 Mineralization Pathways and Phosphorus Retention upon Bioreduction. *Dev. in*
1030 *Earth & Env. Sci.* **7**, 321-348.
1031 Boston P. J., Ivanov M. V. and P. McKay C. (1992) On the possibility of chemosynthetic
1032 ecosystems in subsurface habitats on Mars. *Icarus* **95**, 300–308.
1033 Boyd E.S., Cummings D.C and Geesey G.G. (2007) Mineralogy influences structure and
1034 diversity of bacterial communities associated with geological substrata in a pristine
1035 aquifer. *Microb. Ecol.* **54**, 170-182.
1036 Cabrol N. A., Wynn-Williams D. D., Crawford D. A. and Grin E. A. (2001) Recent
1037 aqueous environments in martian impact craters: An astrological perspective. *Icarus*
1038 **154**, 98–112.
1039 Canfield D. E., Thamdrup B. and Hansen J. W. (1993) The anaerobic degradation of
1040 organic matter in Danish coastal sediments: Iron reduction, manganese reduction,
1041 and sulfate reduction. *Geochim. Cosmochim. Acta* **57**, 3867–3883.
1042 Celi L., Barberis E. and Marsan F. A. (2000) Sorption of phosphate on goethite at high
1043 concentrations. *Soil Sc.* **165**(8), 657-664.
1044 Choi W. K. (2014) Investigations of quantitative reducibility determination and
1045 reducibility variations of neutral hydrogen-dissolved water by electrochemical
1046 analysis. *Int. J. Electrochem. Sci.* **9**, 7266–7276.
1047 Colman D. R., Poudel S., Hamilton T. L., Havig J. R., Selensky M. J., Shock E. L. and
1048 Boyd E. S. (2018) Geobiological feedbacks and the evolution of thermoacidophiles.
1049 *ISME J.* **12**, 225–236.
1050 Cornell R. M. and Schwertmann U. (2003) Iron Oxides: Structure, Property, Reactions,
1051 Occurrences and Uses. 2nd ed., WILEY-VCH GmbH & Co. KGaA, Weinheim.
1052 Crosby H. A., Johnson C. M., Roden E. E. and Beard B. L. (2005) Coupled Fe (II) - Fe
1053 (III) electron and atom exchange as a mechanism for Fe isotope fractionation during
1054 dissimilatory iron oxide reduction. *Environ. Sci. Technol.* **39**, 6698–6704.
1055 Crosby H. A., Roden E. E., Johnson C. M. and Beard B. L. (2007) The mechanisms of

1056 iron isotope fractionation produced during dissimilatory Fe(III) reduction by
1057 *Shewanella putrefaciens* and *Geobacter sulfurreducens*. *Geobiology* **5**, 169–189.
1058 Cwiertny D. M., Handler R. M., Schaefer M. V., Grassian V. H. and Scherer M. M.
1059 (2008) Interpreting nanoscale size-effects in aggregated Fe-oxide suspensions:
1060 Reaction of Fe(II) with Goethite. *Geochim. Cosmochim. Acta* **72**, 1365–1380.
1061 Available at: http://dx.doi.org/10.1016/j.gca.2007.12.018.
1062 Dauphas N., Roskosz M., Alp E. E., Golden D. C., Sio C. K., Tissot F. L. H., Hu M. Y.,
1063 Zhao J., Gao L. and Morris R. V. (2012) A general moment NRIXS approach to the
1064 determination of equilibrium Fe isotopic fractionation factors: Application to
1065 goethite and jarosite. *Geochim. Cosmochim. Acta* **94,** 254–275.
1066 Domagal-Goldman S.D. and Kubicki J.D. (2008) Density functional theory predictions of
1067 equilibrium isotope fractionation of iron due to redox changes and organic
1068 complexation. *Geochim. Cosmochim. Acta* **72**, 5201-5216.
1069 Essington M. E. and Stewart M. A. (2018) Adsorption of Antimonate, Sulfate, and
1070 Phosphate by Goethite: Reversibility and Competitive Effects. *Soil Sci. Soc. Am. J.*
1071 **82**, 803–814.
1072 Fox L. E. (1988) The solubility of colloidal ferric hydroxide and its relevance to iron
1073 concentration in river water. *Geochim. Cosmochim. Acta* **52,** 771–777.
1074 Fernández-Remolar D. C., Morris R. V., Gruener J. E., Amils R. and Knoll A. H. (2005)
1075 The Río Tinto Basin, Spain: Mineralogy, sedimentary geobiology, and implications
1076 for interpretation of outcrop rocks at Meridiani Planum, Mars. *Earth Planet. Sci.*
1077 *Lett.* **240**, 149–167.
1078 Fredrickson J. K., Romine M. F., Beliaev A. S., Auchtung J. M., Driscoll M. E., Gardner
1079 T. S., Nealson K. H., Osterman A. L., Pinchuk G., Reed J. L., Rodionov D. A.,
1080 Rodrigues J. L. M., Saffarini D. A., Serres M. H., Spormann A. M., Zhulin I. B. and
1081 Tiedje J. M. (2008) Towards environmental systems biology of *Shewanella*. *Nat.*
1082 *Rev. Microbiol*. **6**, 592–603.
1083 Fredrickson J.K., Kota S., Kukkadapu R.K., Liu C. and Zachara J. M. (2003) Influence of
1084 Electron Donor/Acceptor Concentrations on Hydrous Ferric Oxide (HFO)
1085 Bioreduction. *Biodegradation* **14,** 91–103. Available at:
1086 https://doi.org/10.1023/A:1024001207574
1087 Frierdich Andrew J, Beard B. L., Reddy T. R., Scherer M. M. and Johnson C. M. (2014a)
1088 Iron isotope fractionation between aqueous Fe (II) and goethite revisited : New
1089 insights based on a multi-direction approach to equilibrium and isotopic exchange
1090 rate modification. *Geochim. Cosmochim. Acta* **139**, 383–398. Available at:
1091 http://dx.doi.org/10.1016/j.gca.2014.05.001.
1092 Frierdich A. J., Beard B. L., Scherer M. M. and Johnson C. M. (2014b) Determination of
1093 the $Fe(II)_{aq}$-magnetite equilibrium iron isotope fractionation factor using the three-
1094 isotope method and a multi-direction approach to equilibrium. *Earth Planet Sci.*
1095 *Lett.* **391**, 77–86.
1096 Geelhoed J. S., Hiemstra T. and Van Riemsdijk W. H. (1997) Phosphate and sulfate
1097 adsorption on goethite: Single anion and competitive adsorption. *Geochim.*
1098 *Cosmochim. Acta* **61**, 2389–2396.
1099 Gu C., Wang Z., Kubicki J. D., Wang X. and Zhu M. (2016) X-ray Absorption
1100 Spectroscopic Quantification and Speciation Modeling of Sulfate Adsorption on
1101 Ferrihydrite Surfaces. *Environ. Sci. Technol.* **50**, 8067–8076.

1102 Handler R. M., Beard B. L., Johnson C. M. and Scherer M. M. (2009) Atom exchange
1103 between aqueous Fe (II) and goethite : An Fe isotope tracer study. *Environ. Sci.*
1104 *Technol.* **43**, 1102–1107.
1105 Handler R. M., Frierdich A. J., Johnson C. M., Rosso K. M., Beard B. L., Wang C., Latta
1106 D. E., Neumann A., Pasakarnis T., Premaratne W. A. P. J. and Scherer M. M. (2014)
1107 Fe(II)-catalyzed recrystallization of goethite revisited. *Environ. Sci. Technol*. **48**,
1108 11302–11311.
1109 Hansel C. M., Benner S. G. and Fendorf S. (2005) Competing Fe(II)-induced
1110 mineralization pathways of ferrihydrite. *Environ. Sci. Technol.* **39**, 7147–7153.
1111 Hansel C. M., Benner S. G., Neiss J., Dohnalkova A., Kukkadapu R. K. and Fendorf S.
1112 (2003) Secondary mineralization pathways induced by dissimilatory iron reduction
1113 of ferrihydrite under advective flow. *Geochim. Cosmochim. Acta* **67**, 2977–2992.
1114 Hansel C. M., Benner S. G., Nico P. and Fendorf S. (2004) Structural constraints of ferric
1115 (hydr)oxides on dissimilatory iron reduction and the fate of Fe(II). *Geochim.*
1116 *Cosmochim. Acta* **68**, 3217–3229.
1117 Hassellöv M. and von der Kammer F. (2008) Iron oxides as geochemical nanovectors for
1118 metal transport in soil-river systems. *Elements* **4**, 401–406.
1119 Hiemstra T. (2013) Surface and mineral structure of ferrihydrite. *Geochim. Cosmochim.*
1120 *Acta* **105**, 316–325. Available at: http://dx.doi.org/10.1016/j.gca.2012.12.002.
1121 Holmes D. E., Dang Y., Walker D. J. F. and Lovley D. R. (2016) The electrically
1122 conductive pili of *Geobacter* species are a recently evolved feature for extracellular
1123 electron transfer. *Microb. Genomics* **2**, 1-20. Available at:
1124 http://www.microbiologyresearch.org/content/journal/mgen/10.1099/mgen.0.000072
1125 Horneck G. (2000) The microbial world and the case for Mars. *Planet. Space Sci.* **48**,
1126 1053–1063.
1127 Hurowitz J. A., Fischer W. W., Tosca N. J. and Milliken R. E. (2010) Origin of acidic
1128 surface waters and the evolutionof atmospheric chemistry on early Mars. *Nat.*
1129 *Geosci.* **3**, 323–326.
1130 Hurowitz J. A. and McLennan S. M. (2007) A ~ 3.5 Ga record of water-limited, acidic
1131 weathering conditions on Mars. *Earth Planet. Sci. Lett.* **260**, 432–443.
1132 Icopini G. A., Anbar A. D., Ruebush S. S., Tien M. and Brantley S. L. (2004) Iron
1133 isotope fractionation during microbial reduction of iron: The importance of
1134 adsorption. *Geology* **32**, 205–208.
1135 Iordanova N., Dupuis M. and Rosso K. M. (2005) Charge transport in metal oxides: A
1136 theoretical study of hematite α-Fe_2O_3. *J. Chem. Phys.* **122**, 144305. Available at:
1137 https://doi.org/10.1063/1.1869492.
1138 Jambor J. L. and Dutrizac J. E. (1998) Occurrence and constitution of natural and
1139 synthetic ferrihydrite, a widespread iron oxyhydroxide. *Chem. Rev.* **98**, 2549–2586.
1140 Available at: http://pubs.acs.org/doi/abs/10.1021/cr970105t.
1141 Jang J. H., Dempsey B. A., Catchen G. L. and Burgos W. D. (2003) Effects of Zn(II),
1142 Cu(II), Mn(II), Fe(II), NO_3^-, or SO_4^{2-} at pH 6.5 and 8.5 on transformations of
1143 hydrous ferric oxide (HFO) as evidenced by Mössbauer spectroscopy. *Colloids Surf.*
1144 *A Physicochem. Eng. Asp.* **221**, 55–68.
1145 Johnson C. M., Beard B. L., Roden E. E., Newman D. K. and Nealson K. H. (2004)
1146 Isotopic Constraints on Biogeochemical Cycling of Fe. *Rev. Mineral. Geochemistry*
1147 **55**, 359–408. Available at:

1148 http://rimg.geoscienceworld.org/cgi/doi/10.2138/gsrmg.55.1.359.
1149 Johnson C. M., Roden E. E., Welch S. A. and Beard B. L. (2005) Experimental
1150 constraints on Fe isotope fractionation during magnetite and Fe carbonate formation
1151 coupled to dissimilatory hydrous ferric oxide reduction. *Geochim. Cosmochim. Acta*
1152 **69**, 963–993.
1153 Jones D. L. (1998) Organic acids in the rhizosphere-a critical review. *Plant Soil* **205**, 25-
1154 44.
1155 Jones L.D., Dennis P.G., Owen A.G. and Van Hees P.A.W. (2003) Organic acids
1156 behavior in soils—misconceptions and knowledge gaps. *Plant and Soil* **248**, 31–41.
1157 Jones A. M., Collins R. N., Rose J. and Waite T. D. (2009) The effect of silica and
1158 natural organic matter on the Fe(II)-catalysed transformation and reactivity of
1159 Fe(III) minerals. *Geochim. Cosmochim. Acta* **73**, 4409–4422. Available at:
1160 http://dx.doi.org/10.1016/j.gca.2009.04.025.
1161 Joshi P., Fantle M. S., Larese-Casanova P. and Gorski C. A. (2017) Susceptibility of
1162 goethite to Fe^{2+}-catalyzed recrystallization over time. *Environ. Sci. Technol.* **51**,
1163 11681–11691.
1164 Katz J. E., Zhang X., Attenkofer K., Chapman K. W., Zarzycki P., Rosso K. M., Falcone
1165 R. W., Waychunas G. A., Katz J. E., Zhang X., Attenkofer K., Chapman K. W.,
1166 Frandsen C., Zarzycki P., Rosso K. M., Falcone R. W., Waychunas G. A. and
1167 Gilbert B. (2012) Electron small polarons and their mobility in iron (Oxyhydr) oxide
1168 nanoparticles. *Science* **337**, 1200–1203.
1169 Krishnamurti G. S. R. and Huang P. M. (1990) Spectrophometric determination of Fe(II)
1170 with 2, 4, 6-Tri(20-pyridyl)-1,3, 5-Triazine in the presence of large quantities of
1171 Fe(III) and complexing ions. *Talanta* **37**, 745–748.
1172 Langner H. W., Jackson C. R., McDermott T. R. and Inskeep W. P. (2001) Rapid
1173 oxidation of arsenite in a hot spring ecosystem, Yellowstone National Park. *Environ.*
1174 *Sci. Technol.* **35**, 3302-3309.
1175 Liu F., He J., Colombo C. and Violante A. (1999) Competitive adsorption of sulfate and
1176 oxalate on goethite in the absence or presence of phosphate. *Soil Sci.* **164**, 180–189.
1177 Lloyd J. R. (2003) Microbial reduction of metals and radionuclides. *FEMS Microbiol.*
1178 *Rev.* **27**, 411–425.
1179 Lovley D. R. (2012) Long-range electron transport to Fe(III) oxide via pili with metallic-
1180 like conductivity. *Biochem. Soc. Trans.* **40**, 1186–1190. Available at:
1181 http://biochemsoctrans.org/lookup/doi/10.1042/BST20120131.
1182 Lovley D. R., Holmes D. E. and Nevin K. P. (2004) Dissimilatory Fe(III) and Mn(IV)
1183 reduction. *Adv. Microb. Physiol.* **49**, 219–286. Available at:
1184 https ://doi.org/10.1016/S0065 -2911(04)49005 -5
1185 Lovley D. R. and Phillips E. J. P. (1986) Organic-matter mineralization with reduction of
1186 ferric iron in anaerobic sediments. *Appl. Environ. Microbiol.* **51**, 683–689.
1187 Mallet M., Barthélémy K., Ruby C., Renard A. and Naille S. (2013) Investigation of
1188 phosphate adsorption onto ferrihydrite by X-ray Photoelectron Spectroscopy. *J.*
1189 *Colloid Interface Sci.* **407**, 95–101. Available at:
1190 http://dx.doi.org/10.1016/j.jcis.2013.06.049.
1191 Millero F.J. (1985) The effect of ionic interactions on the oxidation of metals in natural
1192 waters. *Geochim. Cosmochim. Acta* **49**, 547–553.
1193 Morgan B. and Lahav O. (2007) The effect of pH on the kinetics of spontaneous Fe(II)

oxidation by O2 in aqueous solution - basic principles and a simple heuristic description. *Chemosphere* **68**, 2080–2084.

Morris R. V., Klingelhöfer G., Schröder C., Rodionov D. S., Yen A., Ming D. W., de Souza J. A., Fleischer I., Wdowiak T., Gellert R., Bernhardt B., Evlanov E. N., Zubkov B., Foh J., Bonnes U., Kankeleit E., Gütlich P., Renz F., Squyres S. W. and Arvidson R. E. (2006) Mössbauer mineralogy of rock, soil, and dust at Gusev crater, Mars: Spirit's journey through weakly altered olivine basalt on the plains and pervasively altered basalt in the Columbia Hills. *J. Geophys. Res. E. Planets* **111**, E02S13, Available at: http://dx.doi:10.1029/2005JE002584, 2006

Morris R. V., Klingelhöfer G., Schröer C., Fleischer I., Ming D. W., Yen A. S., Gellert R., Arvidson R. E., Rodionov D. S., Crumpler L. S., Clark B. C., Cohen B. A., McCoy T. J., Mittlefehldt D. W., Schmidt M. E., De Souza J. A. and Squyres S. W. (2008) Iron mineralogy and aqueous alteration from Husband Hill through Home Plate at Gusev Crater, Mars: Results from the Mössbauer instrument on the Spirit Mars Exploration Rover. *J. Geophys. Res. E Planets* **113**, E12S42. Available at: http://dx.doi:10.1029/2008JE003201

Nealson K. H. and Scott J. (2006) Ecophysiology of the genus *Shewanella*. In: Dworkin M, Falkow S., Rosenberg E., Schleifer K.-H., Stackebrandt E. (eds) *Prokaryotes: a handbook on the biology of bacteria*. Springer, New York, 1133–1151.

Nixon S. L., Cousins C. R. and Cockell C. S. (2013) Plausible microbial metabolisms on Mars. *Astron. Geophys*. **54,** 13–16.

Notini L., Byrne J. M., Tomaszewski E. J., Latta D. E., Zhou Z., Scherer M. M. and Kappler A. (2019) Mineral defects enhance bioavailability of goethite toward microbial Fe(III) Reduction. *Environ. Sci. Technol.* **53**, 8883–8891.

Notini L., Latta D. E., Neumann A., Pearce C. I., Sassi M., N'Diaye A. T., Rosso K. M. and Scherer M. M. (2018) The Role of Defects in Fe(II)-Goethite Electron Transfer. *Environ. Sci. Technol.* **52**, 2751–2759.

Odling-Smee J. F., Laland K. N. and Feldman M. W. (1996) Niche Construction. *Am. Nat.* **147**, 641–648.

Pedersen H. D., Postma D., Jakobsen R. and Larsen O. (2005) Fast transformation of iron oxyhydroxides by the catalytic action of aqueous Fe(II). *Geochim. Cosmochim. Acta* **69**, 3967–3977.

Percak-Dennett E. M., Beard B. L., Xu H., Konishi H., Johnson C. M. and Roden E. E. (2011) Iron isotope fractionation during microbial dissimilatory iron oxide reduction in simulated Archaean seawater. *Geobiology* **9**, 205–220.

Percak-Dennett E. M., Loizeau J. L., Beard B. L., Johnson C. M. and Roden E. E. (2013) Iron isotope geochemistry of biogenic magnetite-bearing sediments from the bay of vidy, lake geneva. *Chem. Geol.* **360–361**, 32–40. Available at: http://dx.doi.org/10.1016/j.chemgeo.2013.10.008

Peretyazhko T. S., Niles P. B., Sutter B., Morris R. V., Agresti D. G., Le L. and Ming D. W. (2018) Smectite formation in the presence of sulfuric acid: Implications for acidic smectite formation on early Mars. *Geochim. Cosmochim. Acta* **220**, 248–260.

Reddy T. R., Frierdich A. J., Beard B. L. and Johnson C. M. (2015) The effect of pH on stable iron isotope exchange and fractionation between aqueous Fe(II) and goethite. *Chem. Geol*. **397**, 118–127.

Reguera G., McCarthy K. D., Mehta T., Nicoll J. S., Tuominen M. T. and Lovley D. R.

(2005) Extracellular electron transfer via microbial nanowires. *Nature* **435**, 1098–1101.

Reichard P. U., Kretzschmar R. and Kraemer S. M. (2007) Dissolution mechanisms of goethite in the presence of siderophores and organic acids. *Geochim. Cosmochim. Acta* **71**(23), 5635-5650.

Roden E. E. and Zachara J. M. (1996) Microbial reduction of crystalline iron(III) oxides: Influence of oxide surface area and potential for cell growth. *Environ. Sci. Technol.* **30**, 1618–1628.

Rosso K. M., Smith D. M. A. and Dupuis M. (2003) An *ab initio* model of electron transport in hematite (α-Fe_2O_3) basal planes. *J. Chem. Phys.* **118**, 6455–6466.

Schulthess C. P. and Ndu U. (2017) Modeling the adsorption of hydrogen, sodium, chloride and phthalate on goethite using a strict charge-neutral ion-exchange theory. *PLoS One* **12**, 1–21.

Shi L., Dong H., Reguera G., Beyenal H., Lu A., Liu J., Yu H. Q. and Fredrickson J. K. (2016) Extracellular electron transfer mechanisms between microorganisms and minerals. *Nat. Rev. Microbiol.* **14**, 651–662.

Shi L., Richardson D. J., Wang Z., Kerisit S. N., Rosso K. M., Zachara J. M. and Fredrickson J. K. (2009) The roles of outer membrane cytochromes of *Shewanella* and *Geobacter* in extracellular electron transfer. *Environ. Microbiol. Rep.* **1**, 220–227.

Shi L., Squier T. C., Zachara J. M. and Fredrickson J. K. (2007) Respiration of metal (hydr)oxides by *Shewanella* and *Geobacter*: A key role for multihaem c-type cytochromes. *Mol. Microbiol.* **65**, 12–20.

Shimizu M., Zhou J., Schröder C., Obst M., Kappler A. and Borch T. (2013) Dissimilatory reduction and transformation of ferrihydrite-humic acid coprecipitates. *Environ. Sci. Technol.* **47**, 13375–13384.

Stookey L. L. (1970) Ferrozine-A New Spectrophotometric Reagent for Iron. *Anal. Chem.* **42**, 779–781.

Stumm W. and Morgan J.J. (1996) Aquatic Chemistry: Chemical Equilibria and Rates in Natural Waters. Wiley-Interscience, New York.

Tangalos G. E., Beard B., L., Johnson C. M., Alpers C., N., Shelobolina H. X., Konishi H. and Roden E. E. (2010) Microbial production of isotopically light iron(II) in a modern chemically precipitated sediment and implications for isotopic variations in ancient rocks. *Geobiology* **8**, 197-208.

Taylor S. D., Liu J., Zhang X., Arey B. W., Kovarik L., Schreiber D. K., Perea D. E. and Rosso K. M. (2019) Visualizing the iron atom exchange front in the Fe(II)-catalyzed recrystallization of goethite by atom probe tomography. *Proc. Natl. Acad. Sci. U. S. A.* **116**, 2866-2874.

Vargas M., Kashefi K., Blunt-Harris E. L. and Lovley D. R. (1998) Microbiological evidence for Fe(III) reduction on early earth. *Nature* **395**, 65–67.

Weber K. A., Achenbach L. A. and Coates J. D. (2006) Microorganisms pumping iron: Anaerobic microbial iron oxidation and reduction. *Nat. Rev. Microbiol.* **4**, 752–764.

Welch S. A., Beard B. L., Johnson C. M. and Braterman P. S. (2003) Kinetic and equilibrium Fe isotope fractionation between aqueous Fe(II) and Fe(III). *Geochim. Cosmochim. Acta* **67**, 4231–4250.

Weyer S. and Schwieters J. B. (2003) High precision Fe isotope measurements with high

mass resolution MC-ICPMS. *Int. J. Mass Spectrom*. **226**, 355–368.
Wiederhold J.G., Kraemer S.M., Teutsch N., Borer P.M., Halliday A.N. and Kretzschmar R. (2006) Iron isotope fractionation during proton promoted, ligand controlled, and reductive dissolution of goethite. *Environ. Sci. Technol.* **40**, 3787-3793.
Wiesli R. A., Beard B. L. and Johnson C. M. (2004) Experimental determination of Fe isotope fractionation between aqueous Fe(II), siderite and "green rust" in abiotic systems. *Chem. Geol.* **211**, 343–362.
Williams A. G. B. and Scherer M. M. (2004) Spectroscopic evidence for Fe(II)-Fe(III) electron transfer at the iron oxide-water interface. *Environ. Sci. Technol.* **38**, 4782–4790.
Widdel F., Kohring G.W. and Mayer F. (1983) Studies on dissimilatory sulfate-reducing bacteria that decompose fatty acids. III. Characterization of the filamentous gliding *Desulfonema limicola* gen. nov. sp. nov. and *Desulfonema magnum* sp. nov. *Arch. Microbiol.* **134**(4), 286–294
Wu L., Beard B. L., Roden E. E., Kennedy C. B. and Johnson C. M. (2010) Stable Fe isotope fractionations produced by aqueous Fe(II)-hematite surface interactions. *Geochim. Cosmochim. Acta* **74**, 4249–4265. Available at: http://dx.doi.org/10.1016/j.gca.2010.04.060.
Wu L., Beard B. L., Roden E. E. and Johnson C. M. (2011) Stable iron isotope fractionation between aqueous Fe (II) and hydrous ferric oxide. *Environ. Sci. Technol.* **45,**1847–1852.
Yuwono V. M., Burrows N. D., Soltis J. A., Anh Do T. and Lee Penn R. (2012) Aggregation of ferrihydrite nanoparticles in aqueous systems. *Faraday Discuss.* **159**, 235–245.
Zachara J. M., Fredrickson J. K., Li S. M., Kennedy D. W., Smith S. C. and Gassman P. L. (1998). Bacterial reduction of crystalline Fe^{3+} oxides in single phase suspensions and subsurface materials. *Am. Mineral.* **83**, 1426–1443.
Zhu M., Northrup P., Shi C., Billinge S. J. L., Sparks D. L. and Waychunas G. A. (2014) Structure of Sulfate Adsorption Complexes on Ferrihydrite. *Environ. Sci. Technol. Lett.* **1**, 97–101.

Main Figure Captions

Figure 1. Temporal trends of concentrations of aqueous total Fe, aqueous Fe(II) and Fe(III) in biotic and abiotic dissimilatory iron reduction experiments with ferrihydrite (panels A and C) or goethite (panels B and D). Red squares and blue diamonds represent total Fe_{aq} in biotic and abiotic experiments, respectively. Open and solid symbols in the panels (C) and (D) represent the percentages of Fe(II) and Fe(III) in aqueous Fe, respectively. Error bars representing uncertainty (SD) <2% are not visible in the plot.

Figure 2. Extractable Fe from solids from reactors that contained (A) ferrihydrite and (B) goethite are plotted as a function of time. Fe was extracted using HCl solutions and is presented as the % of total solid Fe used for extraction. Orange and green diamonds represent biotic and abiotic experiments, respectively. Speciation of Fe(II) and Fe(III) in

the extracted Fe from reactors containing (C) ferrihydrite and (D) goethite are plotted against time. Open and solid symbols in the panels (C) and (D) represent the percentages of Fe(II) and Fe(III) in extracted Fe, respectively.

Figure 3. Percentages of total Fe reduction in biotic (black squares) and abiotic (gray circles) reactors containing (A) ferrihydrite and (B) goethite are plotted as a function of time. Percentage of Fe reduction is calculated using total moles of Fe(II) in each reactor relative to the initial moles Fe added to each reactor.

Figure 4. Temporal trends of Fe isotope compositions ($\delta^{56}Fe$) of aqueous total Fe and Fe(II), HCl-extracted total Fe from the solids, and total Fe of the residual solids from biotic (panels A and B) and abiotic (panels C and D) experiments using ferrihydrite and goethite, respevtively. Aqueous Fe(II) (i.e., $Fe(II)_{aq}$) is calculated using measured $\delta^{56}Fe$ values of aqueous total Fe (Eq.3). The solid black lines mark the initial $\delta^{56}Fe$ composition of the stock solids used in these experiments.

Figure 5. High-resolution field emission scanning electron microscopic (FE-SEM) images of pre- and post-incubation (day 19) solids showing no apparent change in the morphology of mineral grains during microbial Fe reduction. Panel (A) and (C) represent pre- and post-incubation ferrihydrite, respectively. Panel (B) and (D) represent pre- and post-incubation goethite. The numbers in the white box at the top right corner in Panel (A) and (B) indicate BET specific surface area (SSA) of the starting ferrihydrite and goethite used for these experiments. The dates on each image represent the date when SEM images were obtained.

Figure 6. Stable Fe isotope fractionation factors between surface reactive Fe(III) (i.e., $Fe(III)_{reac}$) in solids and aqueous Fe(II) ($\Delta^{56}Fe_{Fe(III)reac\text{-}Fe(II)aq}$) are plotted against % Fe reduction from biotic (solid black squares) and abiotic (solid grey circles) experiments. The solid green lines represent equilibrium ferrihydrite-$Fe(II)_{aq}$ ($\Delta^{56}Fe_{Ferrihydrite\text{-}Fe(II)aq}$ = 2.28‰ at 80°C; Wu et al., 2011) and equilibrium goethite-$Fe(II)_{aq}$ ($\Delta^{56}Fe_{Goethite\text{-}Fe(II)aq}$ = 0.73‰ at 80°C; Beard et al., 2010) fractionation factors in panel (A) and panel (B), respectively. The dashed lines represent equilibrium fractionation factors between Fe(III)-oxalate complex and aqueous $[Fe(II)(H_2O)_6]^{2+}$ at 80°C, calculated using In vacuo (1.68‰; dark blue) and IEFPCM (1.41‰; light blue) models (Domagal-Goldman and Kubicki et al., 2008). The solid purple and red lines in panel (B) represent fractionation factors calculated between the reactive surface Fe(III) layer ($\Delta^{56}Fe_{Fe(III)reac\text{-}Fe(II)aq}$) and the aqueous Fe(II) for micro-goethite (μ-Gt: 1.87‰ at 80°C; Crosby et al., 2007) and nano-goethite (η-Gt: 1.47‰ at 80°C; Beard et al., 2010), respectively. The abbreviations Fh and Gt represent ferrihydrite and goethite, respectively.

Figure 7. Fractions of reactive Fe(III) ($X_{Fe(III)reac}$; Eq.7) relative to the total initial Fe in the system are plotted as a function of % Fe reduction of (A) ferrihydrite and (B) goethite in biotic and abiotic experiments. In panel (C) and (D) $X_{Fe(III)reac}$ values are plotted against time for experiments using ferrihydrite and goethite, respectively.

Figure 8. (A) Comparison of stable Fe isotope fractionation factors between Fe in bulk solids (ferrihydrite and goethite) and total dissolved Fe observed in biotic experiments in this study (denoted in figure by "*") and the abiotic dissolution (5 mM oxalate, dark) and reduction (1 mM oxalate, light) experiments by Wiederhold et al. (2006) (denoted in figure by "$"). The experiment durations (time, days) are plotted on the x-axis on a log scale. (B) Stable Fe isotope fractionation factors between $Fe(III)_{reac}$ and $Fe(II)_{aq}$ obtained from ferrihydrite and goethite-bearing biotic reactor in the current study (denoted in figure by "*") are plotted against time (log scale).

Figure 9. Conceptual models for Fe isotope exchange and fractionation between $Fe(II)_{aq}$ and ferric hydroxides during *in situ* (A) abiotic and (B) biotic dissimilatory Fe reduction (DIR) at acidic pH. The mechanism of Fe isotope exchange is illustrated via three stages: [1] Proton-promoted (abiotic) and/or ligand-controlled (biotic) reductive dissolution produces $Fe(II)_{aq}$ near the mineral surface, [2] at the mineral-fluid interface, newly formed $Fe(II)_{aq}$ ions immediately exchange electrons and Fe isotopes with reactive Fe(III) (i.e., $Fe(III)_{reac}$) on the mineral surface resulting in significant $^{56}Fe/^{54}Fe$ fractionation (Δ) between $Fe(III)_{reac}$ and $Fe(II)_{aq}$ ($\Delta^{56}Fe_{Fe(III)_{reac}\text{-}Fe(II)_{aq}}$ (abiotic: 2-2.8‰; biotic: 1.6-2.9‰; see Table 5), and [3] release of $Fe(II)_{aq}$ and some $Fe(III)_{aq}$ (in biotic reactors) into the solution due to acidic pH. The sole source of electrons is H_2 in the headspace. Microbially catalyzed DIR continuously produces $Fe(II)_{aq}$ which promoted extensive Fe isotope exchange leading to the development of a larger fraction of more soluble and distorted $Fe(III)_{reac}$ (i.e., $X_{Fe^{3+}_{reac}} \leq 0.6$) on mineral surfaces compared to that in the abiotic experiments (i.e., $X_{Fe^{3+}_{reac}} \leq 0.09$). Black curved and reversible arrows represent fluxes of $Fe(II)_{aq}$ produced during reductive Fe dissolution on the surface of minerals and Fe isotope exchange, respectively. The thickness of arrows indicates the extent of Fe reduction and Fe isotope exchange. The blue dashed arrow and solid yellow arrow represent dissolution fluxes of $Fe(II)_{aq}$ and $Fe(III)_{aq}$ to the solution at step [3], respectively.

Figure 10. Compilation of the extent of Fe isotope exchange between Fe-oxide minerals (ferrihydrite and goethite) and aqueous Fe(II), represented by %Fe exchanged (from ^{57}Fe-enriched and ^{55}Fe-tracer experiments) or $\%Fe(III)_{reac}$ (from natural Fe isotope exchange experiments) observed in abiotic and biotic systems over various pH conditions in this study and in previous studies, as denoted by symbols following each reference (Crosby et al., 2005[¥], 2007[¶]; Jones et al., 2009[&]; Frierdich et al., 2014a[#]; Handler et al., 2014[§];

1411 Reddy et al., 2015 [$]; Joshi et al., 2017 [¢]). Open and solid symbols represent biotic and
1412 abiotic experiments, respectively. The experiments using freeze-dried samples are listed
1413 as "dried". Data compiled here are from the current and pre-existing experiments with no
1414 or negligible secondary mineral transformation (see Table S.10 for detailed experimental
1415 designs and references).
1416
1417
1418

Paper Tables

Table 1. Definitions of parameters used to describe the experimental results

Parameters	Definitions
Total Fe_{aq} or $Fe_{aq, tot}$	Aqueous total Fe
$Fe(II)_{aq}$	Aqueous Fe(II)
$Fe(III)_{aq}$	Aqueous Fe(III)
$Fe_{extracted}$	HCl-extracted total Fe from solids
$Fe_{residue}$	Total Fe in the solid residue left after HCl-extraction
%Fe reduction	Percent Fe reduction relative to the initial total Fe in the solid substrate
$Fe(III)_{reac}$	Fe(III) in the surface reactive layer of the solid substrate
$X_{Fe(III)reac}$	Fraction $Fe(III)_{reac}$ relative to the initial total Fe in the solid substrate
$X_{Fe(II)extracted}$	Fraction of Fe(II) in the HCl-extracted Fe
$M_{Fe(III)reac}$	total moles of $Fe(III)_{reac}$
$\delta^{56}Fe_{sys}$	Fe isotope composition of the entire system
$\delta^{56}Fe_{aq, tot}$	Fe isotope composition of total aqueous Fe
$\delta^{56}Fe_{extracted}$	Fe isotope composition of total extracted Fe from solid substrate
$\delta^{56}Fe_{residue}$	Fe isotope composition of total Fe in solid residue
$\delta^{56}Fe_{Fe(II)_{aq}}$	Fe isotope composition of $Fe(II)_{aq}$
$\delta^{56}Fe_{Fe(III)_{reac}}$	Fe isotope composition of $Fe(III)_{reac}$
$\delta^{56}Fe_{Fe(II)_{extracted}}$	Fe isotope composition of Fe(II) end-member of the $Fe_{extracted}$
$\delta^{56}Fe_{Fe(II)_{sorbed}}$	Fe isotope composition of sorbed Fe(II)

1422 **Table 2.** Concentration and speciation of Fe in solution from biotic and abiotic experiments with ferrihydrite and goethite

Sample ID	Times (Days)	Solution pH	Total Fe [a] (µM)	SD [a] (µM)	Fe(II) [a] (µM)	SD[a] (µM)	Fe(III) (µM)	SD [a] (µM)	Fe(II) %	Error %	Fe(III) %	Error %
Biotic experiments with ferrihydrite												
Fh-bio-1	2	3.15	22.58	0.03	21.90	0.93	B.D	--	97.00	4.12	--	--
Fh-bio-1’	2	3.15	25.36	0.35	25.00	0.86	B.D	--	98.58	3.65	--	--
Fh-bio-1”	2	3.15	18.89	1.14	18.80	1.27	B.D	--	99.53	9.00	--	--
Fh-bio-2	4	3.15	31.85	0.54	31.85	0.54	B.D	--	100.00	2.38	--	--
Fh-bio-2’	4	3.15	32.46	0.83	32.46	0.83	B.D	--	100.00	3.62	--	--
Fh-bio-2”	4	3.15	37.43	1.52	37.43	1.52	B.D	--	100.00	5.74	--	--
Fh-bio-3	6	3.16	77.87	0.03	77.50	0.55	B.D	--	99.53	0.71	--	--
Fh-bio-3’	6	3.20	61.11	1.19	60.88	1.52	B.D	--	99.62	3.16	--	--
Fh-bio-3”	6	3.20	65.15	1.57	65.00	1.78	B.D	--	99.77	3.64	--	--
Fh-bio-4	10	3.22	91.94	2.17	91.59	2.66	B.D	--	99.62	3.73	--	--
Fh-bio-4’	10	3.22	94.04	0.55	94.04	0.55	B.D	--	100.00	0.82	--	--
Fh-bio-4”	10	3.25	84.61	1.64	84.61	1.64	B.D	--	100.00	2.75	--	--
Fh-bio-5	19	3.28	213.54	0.13	174.66	3.38	38.80	3.26	81.82	1.59	18.21	1.53
Fh-bio-5’	19	3.34	208.43	7.10	164.48	6.70	43.95	0.39	78.91	4.19	21.09	0.74
Fh-bio-5”	19	3.32	218.38	0.14	162.77	1.27	55.61	1.13	74.54	0.58	25.46	0.52
Abiotic experiments with ferrihydrite												
Fh-abio-1	2	3.14	12.71	0.76	12.71	0.76	B.D	--	100.00	8.45	--	--
Fh-abio-2	4	3.13	14.67	0.90	14.67	0.90	B.D	--	100.00	8.66	--	--
Fh-abio-3	6	3.16	12.26	0.64	12.26	0.64	B.D	--	100.00	7.43	--	--
Fh-abio-4	10	3.16	16.58	1.41	16.05	0.67	B.D	--	96.82	9.19	--	--
Fh-abio-5	19	3.16	19.54	1.30	19.54	1.30	B.D	--	100.00	9.40	--	--
Biotic experiments with goethite												
Gt -bio-1	2	3.00	17.99	0.38	19.38	1.58	B.D	--	107.73	9.09	--	--
Gt -bio-1’	2	3.00	14.88	0.27	15.21	0.75	B.D	--	102.25	5.35	--	--
Gt-bio-1”	2	2.99	19.16	1.77	20.32	0.14	B.D	--	106.02	9.82	--	--
Gt -bio-2	4	2.99	28.92	0.13	28.19	0.91	B.D	--	97.76	3.16	--	--

Sample ID	Times (Days)	Solution pH	Total Fe [a] (µM)	SD [a] (µM)	Fe(II) [a] (µM)	SD[a] (µM)	Fe(III) (µM)	SD [a] (µM)	Fe(II) %	Error %	Fe(III) %	Error %
Gt -bio-2'	4	2.98	37.05	0.03	37.03	0.06	B.D	--	99.94	0.17	--	--
Gt -bio-2"	4	2.98	35.01	1.65	35.00	1.65	B.D	--	99.99	6.66	--	--
Gt -bio-3	6	2.99	66.34	0.38	66.36	0.36	B.D	--	100.02	0.79	--	--
Gt -bio-3'	6	2.98	53.59	1.85	52.90	0.86	B.D	--	98.70	3.76	--	--
Gt -bio-3"	6	3.00	64.11	4.05	64.96	2.84	B.D	--	101.33	7.79	--	--
Gt -bio-4	10	3.04	141.67	5.02	124.91	4.16	16.76	0.86	88.17	4.29	11.83	0.74
Gt -bio-4'	10	3.05	138.99	2.32	131.01	1.68	7.98	0.64	94.26	1.98	5.74	0.47
Gt -bio-4"	10	3.04	126.17	4.41	120.62	3.65	5.55	0.76	95.60	4.42	4.40	0.62
Gt -bio-5	19	3.18	362.55	15.53	237.37	16.31	125.18	0.78	65.47	5.30	34.53	1.49
Gt-bio-5'	19	3.20	429.95	4.30	281.22	2.66	148.72	1.64	65.41	0.90	34.59	0.51
Gt-bio-5"	19	3.21	426.37	0.77	286.95	0.37	139.42	0.40	67.30	0.15	32.70	0.11
Abiotic experiments with goethite												
Gt-abio-1	2	2.99	17.55	1.27	17.66	1.10	B.D	--	100.66	9.60	B.D	--
Gt -abio-2	4	2.98	21.50	1.25	21.31	1.52	0.19	0.27	99.11	9.11	0.89	1.26
Gt -abio-3	6	3.00	13.79	0.51	13.80	0.52	B.D	--	100.06	5.26	B.D	--
Gt -abio-4	10	2.99	15.94	1.01	15.89	1.08	B.D	--	99.71	9.27	B.D	--
Gt -abio-5	19	2.99	16.65	0.51	16.86	0.22	B.D	--	101.24	3.34	B.D	--

[a] Fe concentration is measured for 60 ml of solution. The Fe concentration and respective uncertainty represent the calculated average of Fe concentrations measured at MSU and UW and the standard deviation. Detection limit for Fe concentration analysis by *Ferrozine* method is ~1.8 µM. B.D = below detection limit. The abbreviations "Fh", "Gt", "bio", and "abio" refer to ferrihydrite, goethite, biotic, and abiotic experiments, respectively.

1431 **Table 3.** Concentration and speciation of HCl-extracted Fe and solid residues from biotic and abiotic experiments with ferrihydrite
1432 and goethite

					HCl extracted Fe									Solid residue	
Sample ID	**Times (Days)**	**% Fe extracted from solids**	**Error %**	**Total Fe [a] (µM)**	**SD (µM)**	**Fe(II) [a] (µM)**	**SD (µM)**	**Fe(III) [a] (uM)**	**SD (µM)**	**Fe(II) %**	**Error %**	**Fe(III) %**	**Error %**	**Fe(III) %**	**Error %**
	Biotic experiments with ferrihydrite														
Fh-bio-1	2	0.21	0.01	169.37	1.21	11.01	1.83	158.37	2.20	6.50	1.08	93.50	1.46	99.99	3.37
Fh-bio-1'	2	0.16	0.01	136.76	2.10	31.19	3.67	105.57	4.23	22.80	2.71	77.20	3.31	99.98	4.68
Fh-bio-1"	2														
Fh-bio-2	4	0.15	0.01	123.72	2.10	22.01	1.83	101.70	2.79	17.79	1.51	82.21	2.65	99.98	2.98
Fh-bio-2'	4	0.07	0.01	55.97	3.21	4.92	1.83	51.04	3.70	8.80	3.32	91.20	8.44	99.99	3.33
Fh-bio-2"	4														
Fh-bio-3	6	0.04	0.01	34.61	2.24	3.67	1.34	30.94	2.61	10.60	3.94	89.40	9.50	99.99	4.95
Fh-bio-3'	6	0.09	0.01	71.43	3.21	7.34	1.06	64.09	3.38	10.27	1.55	89.73	6.22	99.98	3.23
Fh-bio-3"	6														
Fh-bio-4	10	0.07	0.01	51.62	1.16	6.67	3.67	44.95	3.85	12.92	7.11	87.08	7.71	99.97	3.37
Fh-bio-4'	10	0.07	0.03	55.23	2.10	6.73	2.80	48.50	3.50	12.18	5.09	87.82	7.17	99.98	3.45
Fh-bio-4"	10														
Fh-bio-5	19														
Fh-bio-5'	19	0.11	0.01	86.16	2.10	8.56	3.67	77.60	4.23	9.94	4.27	90.06	5.38	99.97	6.93
Fh-bio-5"	19	0.11	0.01	86.16	4.21	7.95	1.83	78.21	4.59	9.23	2.18	90.77	6.93	99.97	10.50
	Abiotic experiments with ferrihydrite														
Fh-abio-1	2	0.11	0.01	92.05	3.21	7.34	3.18	84.71	4.52	7.97	3.46	92.03	5.87	99.99	3.22
Fh-abio-2	4	0.09	0.01	77.32	1.21	3.67	1.06	73.65	1.61	4.75	1.37	95.25	2.57	99.99	6.36
Fh-abio-3	6	0.04	0.01	33.87	2.24	2.29	1.07	31.58	2.48	6.77	3.20	93.23	9.57	99.99	3.21
Fh-abio-4	10	0.11	0.01	90.58	2.10	5.50	3.67	85.07	4.23	6.08	4.05	93.92	5.15	99.99	9.05
Fh-abio-5	19	0.09	0.01	68.49	2.10	7.34	1.83	61.15	2.79	10.71	2.70	89.29	4.91	100.00	2.99
	Biotic experiments with goethite														
Gt -bio-1	2	0.67	0.02	511.35	1.25	76.17	1.83	435.18	2.20	14.90	0.36	85.10	0.48	99.99	3.22
Gt -bio-1'	2	0.67	0.01	500.06	1.25	73.38	1.83	426.68	2.20	14.67	0.37	85.33	0.49	99.99	3.06
Gt-bio-1"	2														
Gt -bio-2	4	0.49	0.01	367.78	2.06	14.68	1.83	353.11	2.79	3.99	0.50	96.01	0.93	99.99	3.40
Gt -bio-2'	4	0.56	0.01	417.79	1.25	47.70	1.83	370.09	2.20	11.42	0.44	88.58	0.59	99.98	2.97
Gt -bio-2"	4														

				HCl extracted Fe										Solid residue	
Sample ID	**Times (Days)**	**% Fe extracted from solids**	**Error %**	**Total Fe [a] (µM)**	**SD (µM)**	**Fe(II) [a] (µM)**	**SD (µM)**	**Fe(III) [a] (uM)**	**SD (µM)**	**Fe(II) %**	**Error %**	**Fe(III) %**	**Error %**	**Fe(III) %**	**Error %**
Gt -bio-3	6	0.61	0.01	443.60	1.25	31.80	4.62	411.80	4.77	7.17	1.04	92.83	1.11	99.98	2.75
Gt -bio-3'	6	0.46	0.01	351.65	1.25	19.57	2.80	332.09	3.05	5.56	0.80	94.44	0.93	99.98	2.68
Gt -bio-3"	6														
Gt -bio-4	10	0.71	0.02	525.87	1.25	19.57	2.80	506.30	3.05	3.72	0.53	96.28	0.62	99.98	3.34
Gt -bio-4'	10	0.68	0.02	504.90	6.45	25.68	1.83	479.21	6.68	5.09	0.37	94.91	1.79	99.97	2.93
Gt -bio-4"	10														
Gt -bio-5	19	0.89	0.01	601.68	1.25	18.35	1.93	583.34	2.28	3.05	0.32	96.95	0.43	99.98	2.28
Gt-bio-5'	19	1.0	0.02	679.11	2.42	31.80	1.06	647.31	2.65	4.68	0.16	95.32	0.52	99.98	2.83
Gt-bio-5"	19														
	Abiotic experiments with goethite														
Gt-abio-1	2	0.59	0.01	472.64	2.42	13.76	1.83	458.88	3.04	2.91	0.39	97.09	0.81	100.00	3.14
Gt -abio-2	4	0.53	0.01	427.47	1.25	14.68	1.83	412.79	2.20	3.43	0.43	96.57	0.59	100.00	3.20
Gt -abio-3	6	0.58	0.01	467.80	3.22	14.68	1.83	453.12	3.70	3.14	0.39	96.86	1.04	100.00	3.22
Gt -abio-4	10	1.11	0.03	887.90	2.06	18.35	2.80	869.56	3.50	2.07	0.32	97.93	0.46	99.99	3.31
Gt -abio-5	19	0.43	0.01	343.59	2.06	11.01	1.06	332.58	2.36	3.20	0.31	96.80	0.90	99.99	3.09

[a] Fe concentration is measured for 2 ml of HCl-extracts. Detection limit for Fe concentration analysis by *Ferrozine* method is ~1.8 µM. B.D = below detection limit. The abbreviations "Fh", "Gt", "bio", and "abio" refer to ferrihydrite, goethite, biotic, and abiotic experiments, respectively.

Table 4. Measured Fe isotopic ($\delta^{56}Fe$) compositions of total Fe in solution, HCl-extracts, and solid residues from biotic and abiotic experiments with ferrihydrite and goethite

Sample ID	**Times (Days)**	**Aqueous total Fe**	**Extracted total Fe**	**Residue total Fe in solids**
		$\delta^{56}Fe_{aq,\ tot}$ ‰	**$\delta^{56}Fe_{extracted}$ ‰**	**$\delta^{56}Fe_{residue}$ ‰**
	Biotic experiments with ferrihydrite			
Fh-bio-1	2	-2.64 (0.21)	-0.01 (0.09)	0.12
Fh-bio-1'	2	-2.59 (0.10)	-0.24 (0.09)	0.04

Sample ID	Times (Days)	Aqueous total Fe	Extracted total Fe	Residue total Fe in solids
		$\delta^{56}Fe_{aq, tot}$ ‰	$\delta^{56}Fe_{extracted}$ ‰	$\delta^{56}Fe_{residue}$ ‰
Fh-bio-1”	2	-2.69 (0.07)		
Fh-bio-2	4	-2.46 (0.25)	0.04 (0.19)	-0.10
Fh-bio-2’	4	-2.54 (0.13)	0.22 (0.07)	0.07
Fh-bio-2”	4	-2.49 (0.04)		
Fh-bio-3	6	-2.36 (0.03)	0.11 (0.05)	-0.13
Fh-bio-3’	6	-2.55 (0.10)	0.25 (0.04)	0.02
Fh-bio-3”	6	-2.52 (0.01)		
Fh-bio-4	10	-2.37 (0.10)	-0.10	0.07
Fh-bio-4’	10	-2.30 (0.07)		0.22
Fh-bio-4”	10	-2.38 (0.04)		
Fh-bio-5	19	-2.64 (0.06)		
Fh-bio-5’	19	-2.08 (0.06)	0.03 (0.06)	0.41
Fh-bio-5”	19	-2.11 (0.07)	0.14	0.26
	Abiotic experiments with ferrihydrite			
Fh-abio-1	2	-2.63 (0.10)	-0.03	0.08 (0.03)
Fh-abio-2	4	-2.65 (0.14)	0.13	0.04 (0.20)
Fh-abio-3	6	-2.69 (0.10)	0.02	0.04 (0.04)
Fh-abio-4	10	-2.12 (0.05)	0.16	0.05 (0.13)
Fh-abio-5	19	-2.74	-0.04	-0.01 (0.07)
	Biotic experiments with goethite			
Gt -bio-1	2	-1.09 (0.08)	0.35 (0.08)	0.04 (0.10)
Gt -bio-1’	2	-1.03 (0.05)	0.36 (0.09)	0.01
Gt-bio-1”	2	-0.96 (0.04)		
Gt -bio-2	4	-0.88 (0.02)	0.65 (0.08)	-0.03
Gt -bio-2’	4	-0.82 (0.05)	0.67 (0.02)	0.03
Gt -bio-2”	4	-0.77 (0.06)		
Gt -bio-3	6	-0.56 (0.05)	0.76 (0.13)	0.03
Gt -bio-3’	6	-0.68 (0.05)		0.06
Gt -bio-3”	6	-0.76 (0.03)		
Gt -bio-4	10	-0.31 (0.05)	0.74 (0.06)	0.04
Gt -bio-4’	10	-0.34 (0.14)	0.84 (0.02)	0.05
Gt -bio-4”	10	-0.35 (0.18)		

Sample ID	Times (Days)	Aqueous total Fe	Extracted total Fe	Residue total Fe in solids
		$\delta^{56}Fe_{aq,\,tot}$ ‰	$\delta^{56}Fe_{extracted}$ ‰	$\delta^{56}Fe_{residue}$ ‰
Gt -bio-5	19	-0.16 (0.08)	0.78 (0.05)	0.00
Gt-bio-5’	19	-0.13 (0.11)	0.80 (0.12)	0.05
Gt-bio-5”	19	-0.16 (0.05)		
	Abiotic experiments with goethite			
Gt-abio-1	2	-1.19 (0.11)	0.43 (0.13)	-0.01
Gt -abio-2	4	-1.28 (0.01)	0.50 (0.03)	-0.01
Gt -abio-3	6	-1.57 (.06)	0.41	0.11
Gt -abio-4	10	-1.61 (0.01)	0.52	0.02
Gt -abio-5	19	-1.58 (0.03)	0.61 (0.02)	0.04

Long-term analytical precision (2SD) for $\delta^{56}Fe$ is 0.08‰. Values within parentheses represent 2 standard deviations of the average value of the samples that were analyzed 2-3 times. The abbreviations “Fh”, “Gt”, “bio”, and “abio” refer to ferrihydrite, goethite, biotic, and abiotic experiments, respectively.

Table 5. Parameters derived from measured Fe concentrations and isotope compositions ($\delta^{56}Fe$) of solids, fluids, and extracted Fe from biotic and abiotic experiments with ferrihydrite and goethite

Sample ID	Time (Days)			Aqueous ferrous Fe $(Fe(II)_{aq})$		Reactive Fe(III) $(Fe(III)_{reac})$		$\Delta^{56}Fe_{Fe(III)_{reac}-Fe(II)_{aq}}$		Fraction of reactive Fe(III)		Fraction of Fe(II) incorporated in solids	$\Delta^{56}Fe_{Fe_{extracted}-Fe(II)_{aq}}$	
		%Fe reduction	Error [a] %	$\delta^{56}Fe$ ‰	Error [b] ‰	$\delta^{56}Fe$ ‰	Error [b] ‰	‰	Error [b] ‰	$X_{Fe(III)reac}$	Error [a] ‰	%	‰	Error [b] ‰
	Biotic experiments with ferrihydrite													
Fh-bio-1	2	0.85	0.05	-2.73	0.32	0.14	0.11	2.87	0.34	0.16	0.03	3.24	2.72	0.34
Fh-bio-1’	2	0.97	0.05	-2.63	0.15	0.30	0.20	2.92	0.25	0.08	0.01	6.19	2.38	0.18
Fh-bio-1”	2	0.68	0.05	-2.70	0.08									
Fh-bio-2	4	1.22	0.04	-2.46	0.25	0.47	0.25	2.93	0.35	0.06	0.01	3.70	2.51	0.31
Fh-bio-2’	4	1.20	0.04	-2.54	0.13	0.43	0.20	2.98	0.23	0.07	0.01	1.24	2.76	0.14
Fh-bio-2”	4	1.36	0.07	-2.49	0.04									

Sample ID	Time (Days)			Aqueous ferrous Fe ($Fe(II)_{aq}$)		Reactive Fe(III) ($Fe(III)_{reac}$)		$\Delta^{56}Fe_{Fe(III)_{reac}-Fe(II)_{aq}}$		Fraction of reactive Fe(III)		Fraction of Fe(II) incorporated in solids	$\Delta^{56}Fe_{Fe_{extracted}-Fe(II)_{aq}}$	
		%Fe reduction	Error [a] %	$\delta^{56}Fe$ ‰	Error [b] ‰	$\delta^{56}Fe$ ‰	Error [b] ‰	‰	Error [b] ‰	$X_{Fe(III)reac}$	Error [a] ‰	%	‰	Error [b] ‰
Fh-bio-3	6	2.83	0.10	-2.37	0.05	0.34	0.21	2.71	0.22	0.20	0.02	0.63	2.48	0.07
Fh-bio-3’	6	2.25	0.08	-2.56	0.10	0.51	0.10	3.06	0.14	0.11	0.01	1.39	2.81	0.11
Fh-bio-3”	6	2.37	0.11	-2.53	0.02									
Fh-bio-4	10	3.40	0.13	-2.38	0.10	0.15	0.34	2.53	0.36	0.52	0.06	1.03	2.28	0.13
Fh-bio-4’	10	3.45	0.09	-2.30	0.07									
Fh-bio-4”	10	3.08	0.13	-2.38	0.04									
Fh-bio-5	19	6.36	0.26	-3.17	0.11									
Fh-bio-5’	19	5.98	0.36	-2.69	0.08	0.27	0.23	2.95	0.24	0.62	0.08	0.62	2.71	0.10
Fh-bio-5”	19	5.97	0.41	-2.84	0.08	0.39	0.16	3.23	0.18	0.45	0.06	0.68	2.98	0.11
	Abiotic experiments with ferrihydrite													
Fh-abio-1	2	0.47	0.05	-2.63	0.10	0.14	0.20	2.77	0.22	0.09	0.01	3.17	2.60	0.13
Fh-abio-2	4	0.53	0.07	-2.65	0.14	0.24	0.11	2.89	0.18	0.06	0.01	2.20	2.77	0.17
Fh-abio-3	6	0.45	0.04	-2.69	0.10	0.17	0.21	2.86	0.23	0.07	0.01	2.55	2.71	0.13
Fh-abio-4	10	0.56	0.05	-2.21	0.25	0.27	0.18	2.49	0.30	0.04	0.01	2.60	2.37	0.26
Fh-abio-5	19	0.74	0.05	-2.74	0.10	0.22	0.17	2.96	0.20	0.09	0.01	1.84	2.70	0.13
	Biotic experiments with goethite													
Gt -bio-1	2	0.86	0.07	-1.09	0.08	0.46	0.10	1.54	0.13	0.019	0.004	12.30	1.44	0.12
Gt -bio-1’	2	0.71	0.04	-1.03	0.05	0.45	0.11	1.48	0.12	0.014	0.002	14.59	1.39	0.11
Gt-bio-1”	2	0.80	0.01	-0.96	0.04									
Gt -bio-2	4	1.15	0.05	-0.95	0.02	0.68	0.08	1.63	0.09	0.016	0.002	2.96	1.60	0.08
Gt -bio-2’	4	1.54	0.04	-0.83	0.05	0.75	0.02	1.58	0.05	0.016	0.002	5.07	1.50	0.05
Gt -bio-2”	4	1.37	0.07	-0.77	0.06									
Gt -bio-3	6	2.73	0.06	-0.56	0.05	0.79	0.14	1.36	0.15	0.019	0.002	2.26	1.32	0.14
Gt -bio-3’	6	2.08	0.06	-0.72	0.12							2.04		
Gt -bio-3”	6	2.55	0.11	-0.76	0.03									
Gt -bio-4	10	4.80	0.19	-0.65	0.07	0.76	0.06	1.41	0.09	0.047	0.006	0.99	1.39	0.09
Gt -bio-4’	10	5.07	0.12	-0.34	0.14	0.86	0.02	1.20	0.14	0.023	0.009	1.12	1.18	0.14
Gt -bio-4”	10	4.73	0.15	-0.48	0.19									
Gt -bio-5	19	9.11	0.64	-1.15	0.12	0.81	0.05	1.96	0.13	0.177	0.024	0.49	1.93	0.14

Sample ID	Time (Days)			Aqueous ferrous Fe ($Fe(II)_{aq}$)		Reactive Fe(III) ($Fe(III)_{reac}$)		$\Delta^{56}Fe_{Fe(III)_{reac}-Fe(II)_{aq}}$		Fraction of reactive Fe(III)		Fraction of Fe(II) incorporated in solids	$\Delta^{56}Fe_{Fe_{extracted}-Fe(II)_{aq}}$	
		%Fe reduction	Error [a] %	$\delta^{56}Fe$ ‰	Error [b] ‰	$\delta^{56}Fe$ ‰	Error [b] ‰	‰	Error [b] ‰	$X_{Fe(III)reac}$	Error [a] ‰	%	‰	Error [b] ‰
Gt-bio-5’	19	10.47	0.20	-1.13	0.11	0.86	0.13	1.98	0.17	0.192	0.018	0.55	1.93	0.17
Gt-bio-5”	19	11.25	0.08	-1.10	0.05									
	Abiotic experiments with goethite													
Gt-abio-1	2	0.69	0.05	-1.19	0.11	0.45	0.14	1.64	0.18	0.018	0.003	3.17	1.62	0.18
Gt -abio-2	4	0.82	0.06	-1.31	0.02	0.53	0.03	1.84	0.03	0.020	0.003	2.66	1.80	0.03
Gt -abio-3	6	0.58	0.03	-1.54	0.08	0.44	0.01	2.01	0.06	0.020	0.002	3.97	1.98	0.06
Gt -abio-4	10	0.63	0.04	-1.60	0.12	0.55	0.01	2.17	0.01	0.018	0.003	5.26	2.14	0.01
Gt -abio-5	19	0.68	0.02	-1.58	0.15	0.65	0.03	2.23	0.04	0.016	0.001	3.10	2.19	0.04

[a] Errors are represented by % error calculated by propagating the analytical error.

[b] Errors are represented by 2 standard deviations calculated by propagating the analytical error.

The abbreviations “Fh”, “Gt”, “bio”, and “abio” refer to ferrihydrite, goethite, biotic, and abiotic experiments, respectively.

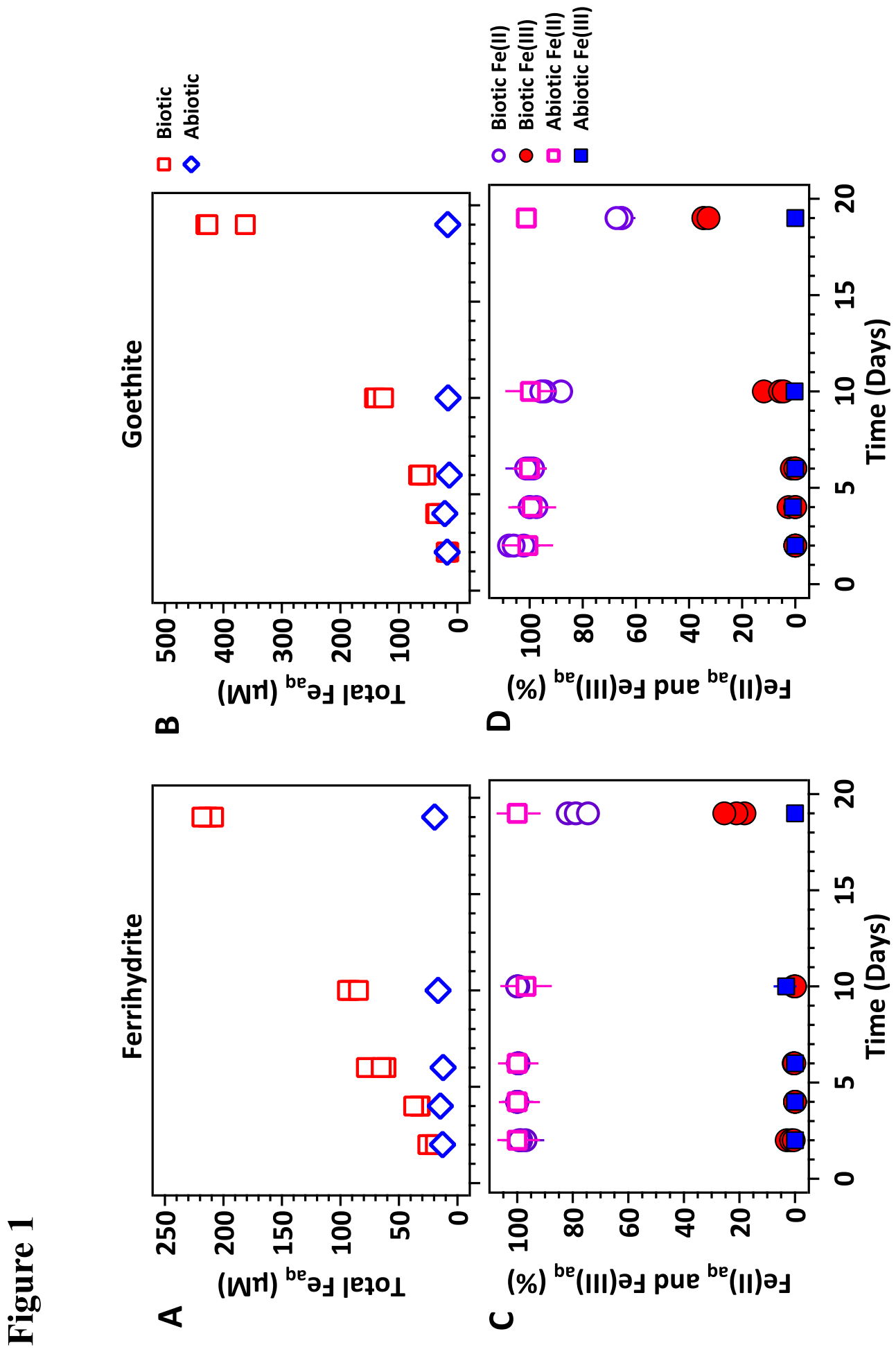
Figure 1
A
Ferrihydrite
Total Fe$_{aq}$ (μM)
250
200
150
100
50
0
B
Goethite
Total Fe$_{aq}$ (μM)
500
400
300
200
100
0
Biotic
Abiotic
C
Fe(II)$_{aq}$ and Fe(III)$_{aq}$ (%)
100
80
60
40
20
0
0
5
10
15
20
Time (Days)
D
Fe(II)$_{aq}$ and Fe(III)$_{aq}$ (%)
100
80
60
40
20
0
0
5
10
15
20
Time (Days)
Biotic Fe(II)
Biotic Fe(III)
Abiotic Fe(II)
Abiotic Fe(III)

Figure 2

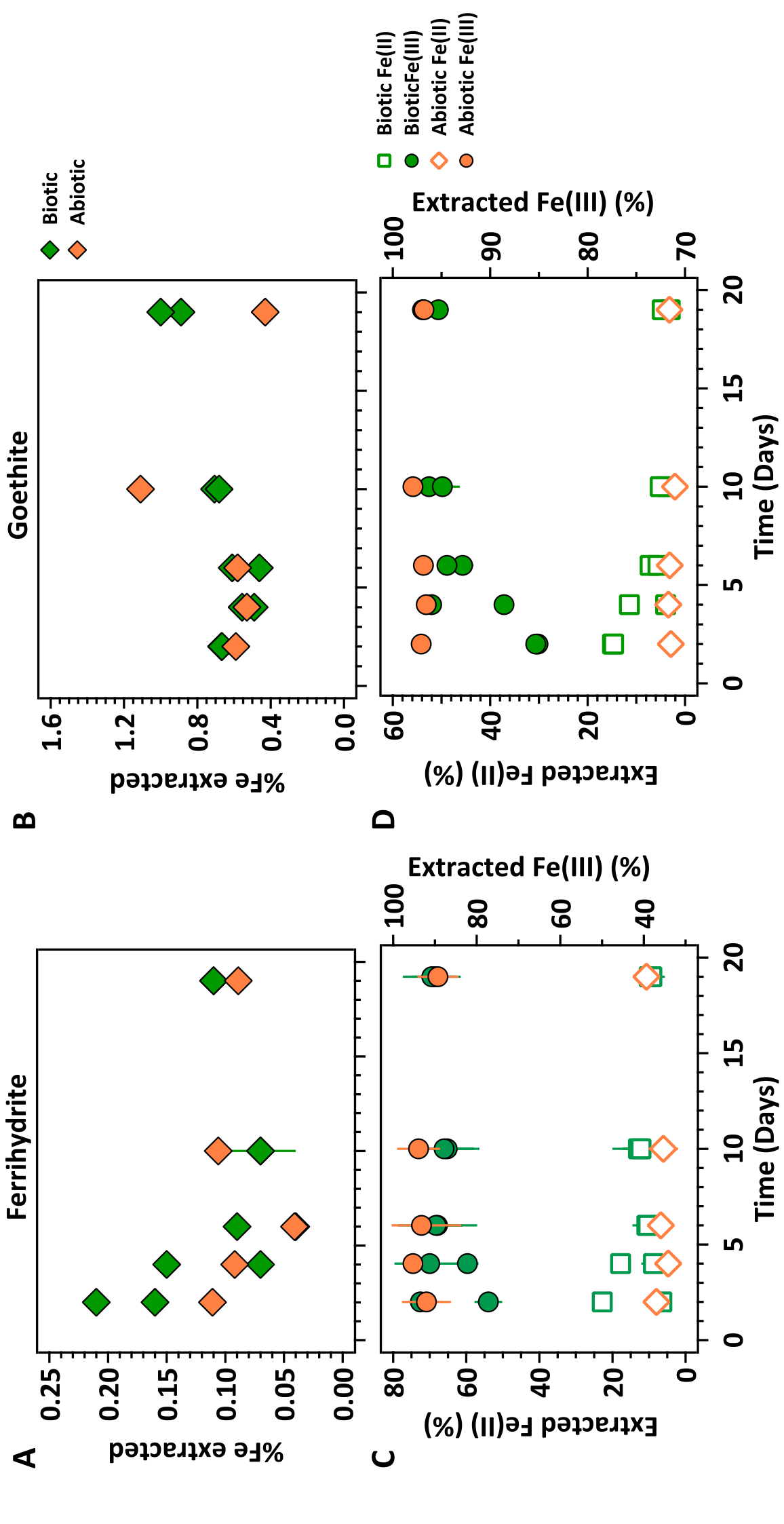
A
Ferrihydrite
%Fe extracted
0.25
0.20
0.15
0.10
0.05
0.00
B
Goethite
%Fe extracted
1.6
1.2
0.8
0.4
0.0
Biotic
Abiotic
C
Extracted Fe(II) (%)
Extracted Fe(III) (%)
Time (Days)
0
5
10
15
20
80
60
40
20
0
100
80
60
40
D
Extracted Fe(II) (%)
Extracted Fe(III) (%)
Time (Days)
60
40
20
0
100
90
80
70
Biotic Fe(II)
BioticFe(III)
Abiotic Fe(II)
Abiotic Fe(III)

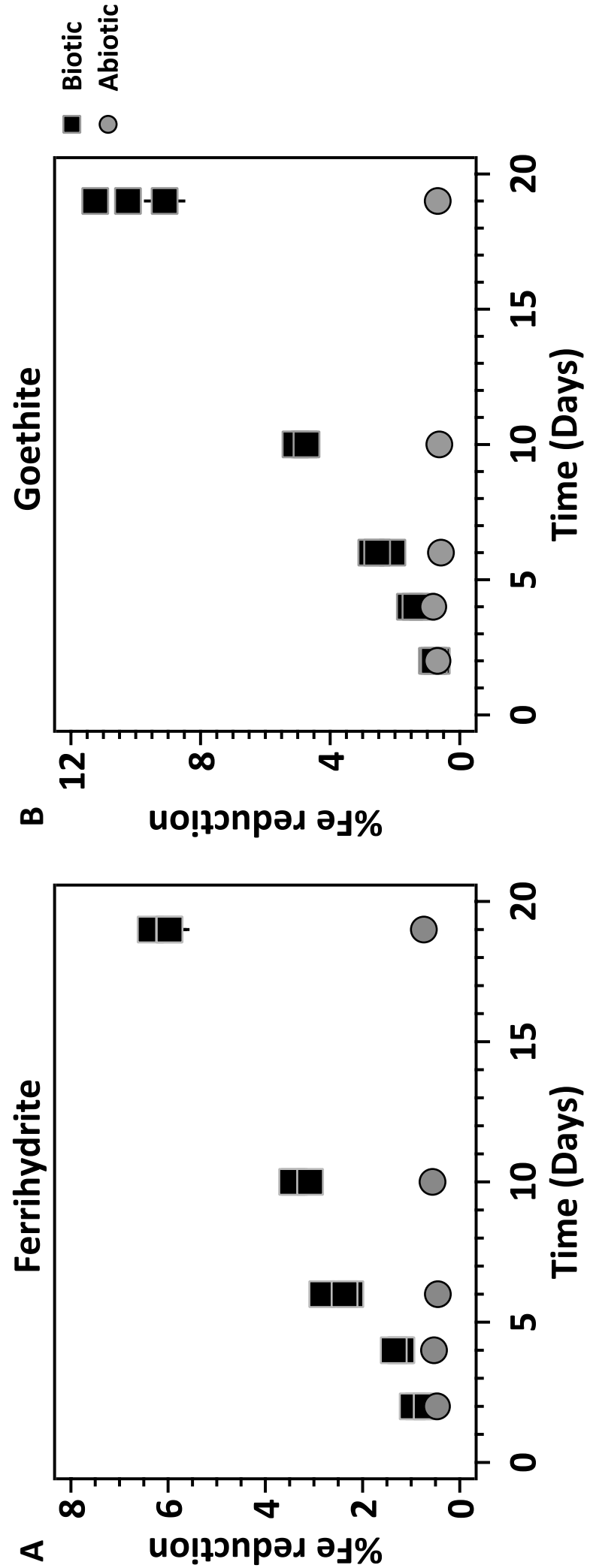
A
Ferrihydrite
%Fe reduction
0
2
4
6
8
0
5
10
15
20
Time (Days)
B
Goethite
%Fe reduction
0
4
8
12
0
5
10
15
20
Time (Days)
Biotic
Abiotic

Figure 3

Figure 4

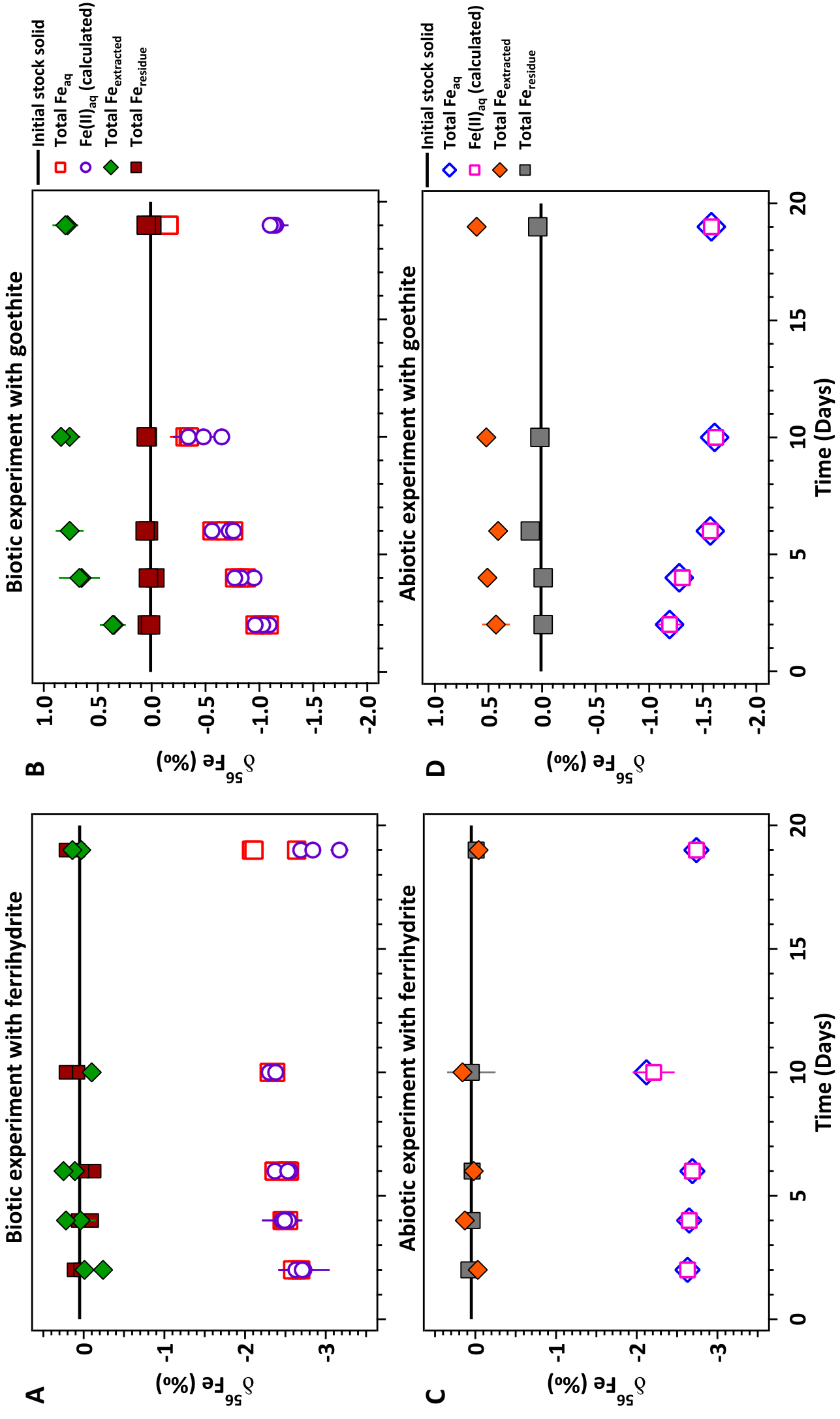

Figure 4

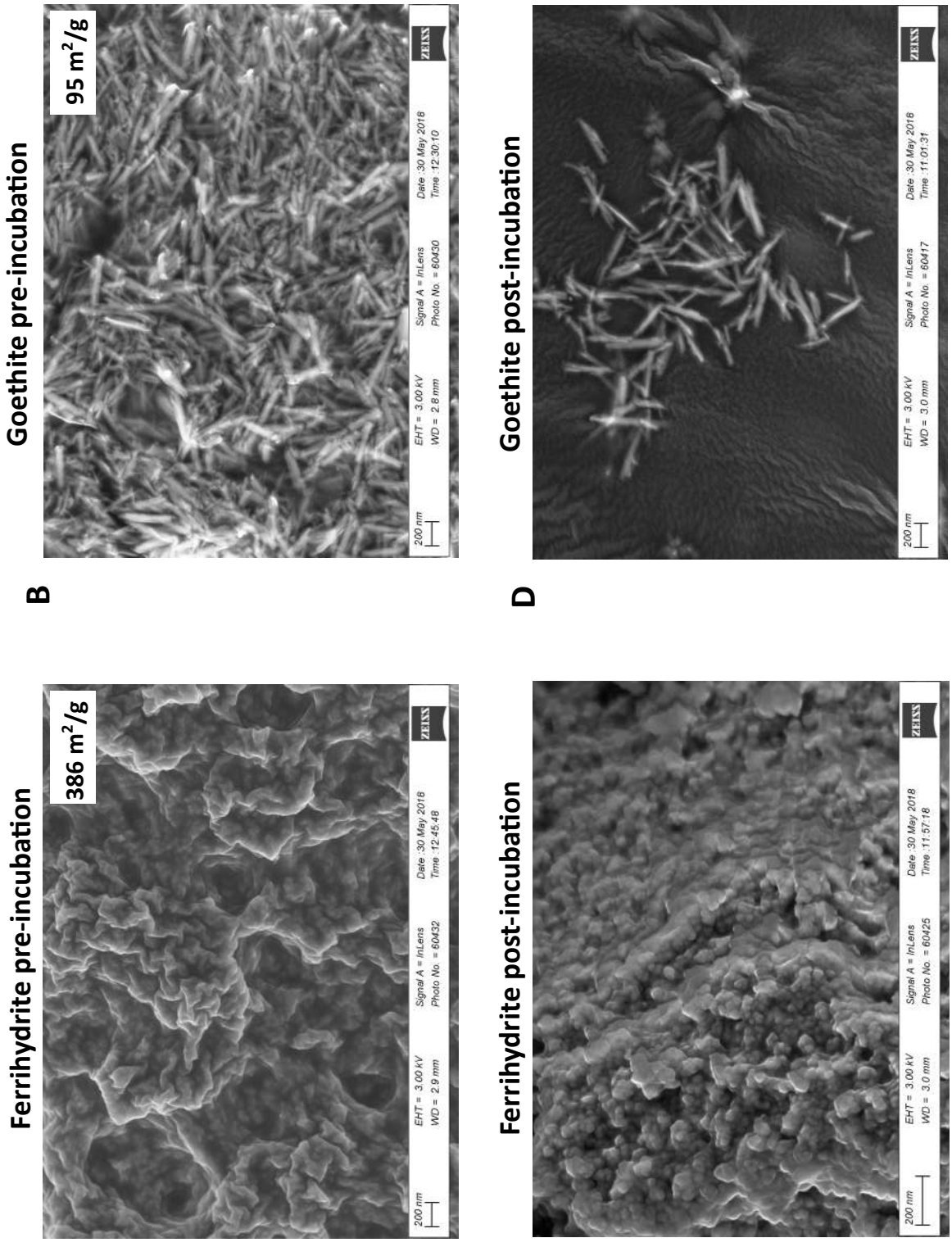
A
Ferrihydrite pre-incubation
386 m²/g
B
Goethite pre-incubation
95 m²/g
C
Ferrihydrite post-incubation
D
Goethite post-incubation
ZEISS

Figure 5

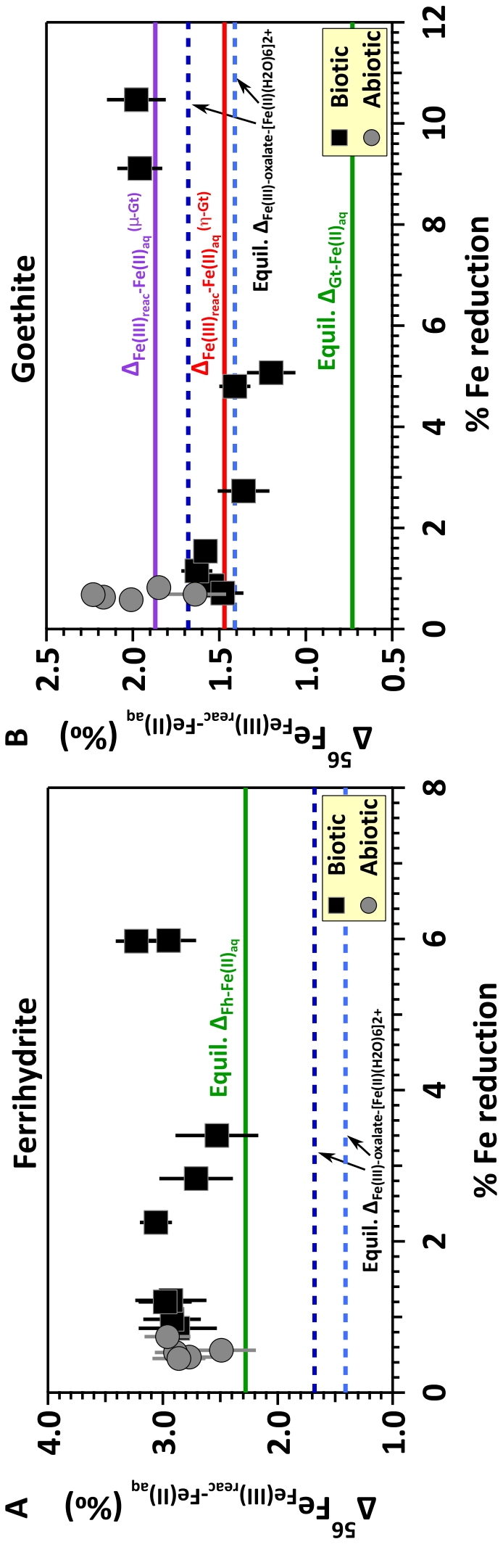
A
Ferrihydrite
$\Delta^{56}Fe_{Fe(III)reac-Fe(II)aq}$ (‰)
Biotic
Abiotic
Equil. $\Delta_{Fh\text{-}Fe(II)aq}$
Equil. $\Delta_{Fe(III)\text{-}oxalate\text{-}[Fe(II)(H2O)6]2+}$
% Fe reduction
B
Goethite
$\Delta^{56}Fe_{Fe(III)reac-Fe(II)aq}$ (‰)
$\Delta_{Fe(III)reac\text{-}Fe(II)aq}$ (μ-Gt)
$\Delta_{Fe(III)reac\text{-}Fe(II)aq}$ (η-Gt)
Equil. $\Delta_{Fe(III)\text{-}oxalate\text{-}[Fe(II)(H2O)6]2+}$
Equil. $\Delta_{Gt\text{-}Fe(II)aq}$
Biotic
Abiotic
% Fe reduction

Figure 6

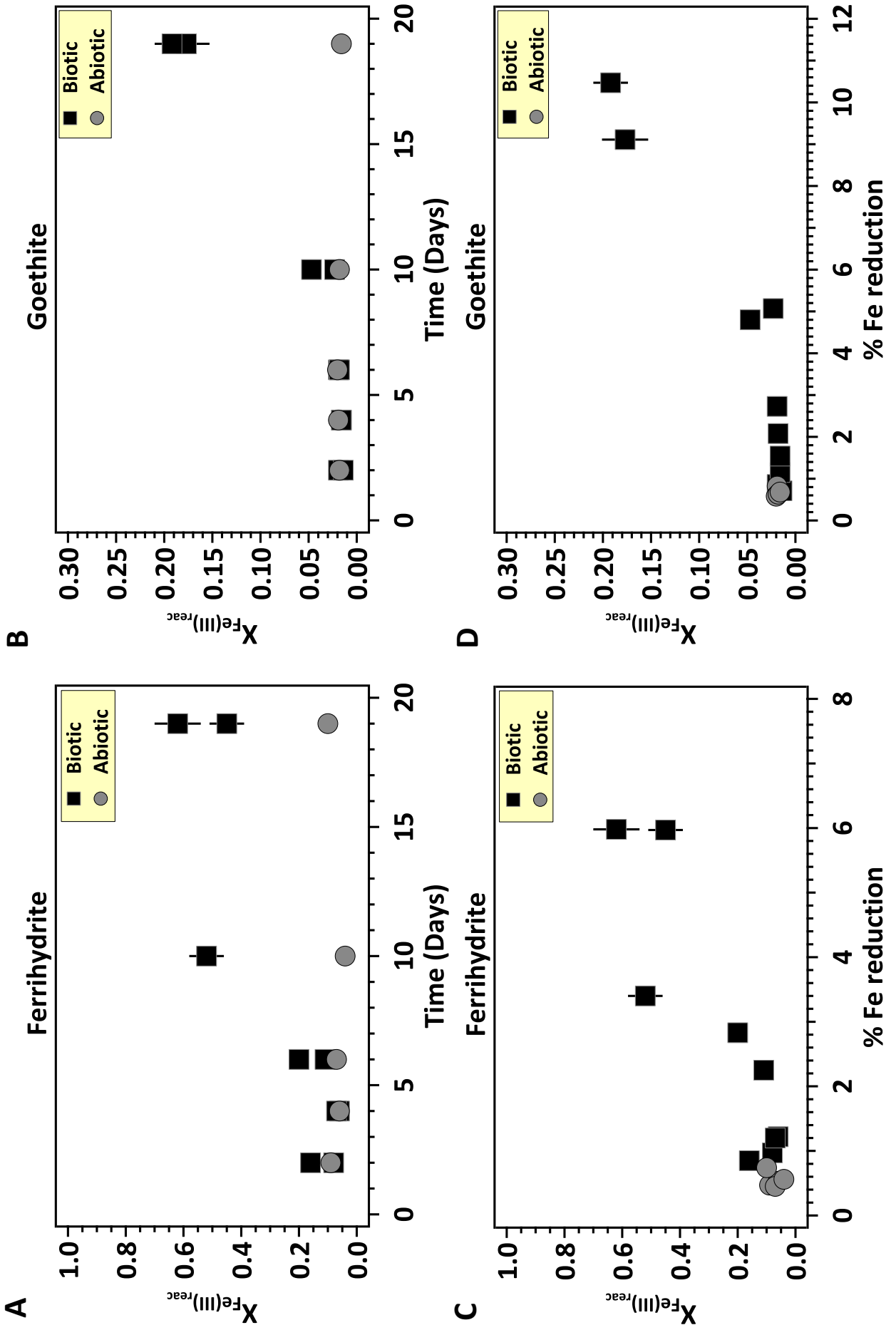
A
Ferrihydrite
Biotic
Abiotic
$X_{Fe(III)reac}$
1.0
0.8
0.6
0.4
0.2
0.0
0
5
10
15
20
Time (Days)
B
Goethite
Biotic
Abiotic
$X_{Fe(III)reac}$
0.30
0.25
0.20
0.15
0.10
0.05
0.00
0
5
10
15
20
Time (Days)
C
Ferrihydrite
Biotic
Abiotic
$X_{Fe(III)reac}$
1.0
0.8
0.6
0.4
0.2
0.0
0
2
4
6
8
% Fe reduction
D
Goethite
Biotic
Abiotic
$X_{Fe(III)reac}$
0.30
0.25
0.20
0.15
0.10
0.05
0.00
0
2
4
6
8
10
12
% Fe reduction

Figure 7

Figure 8

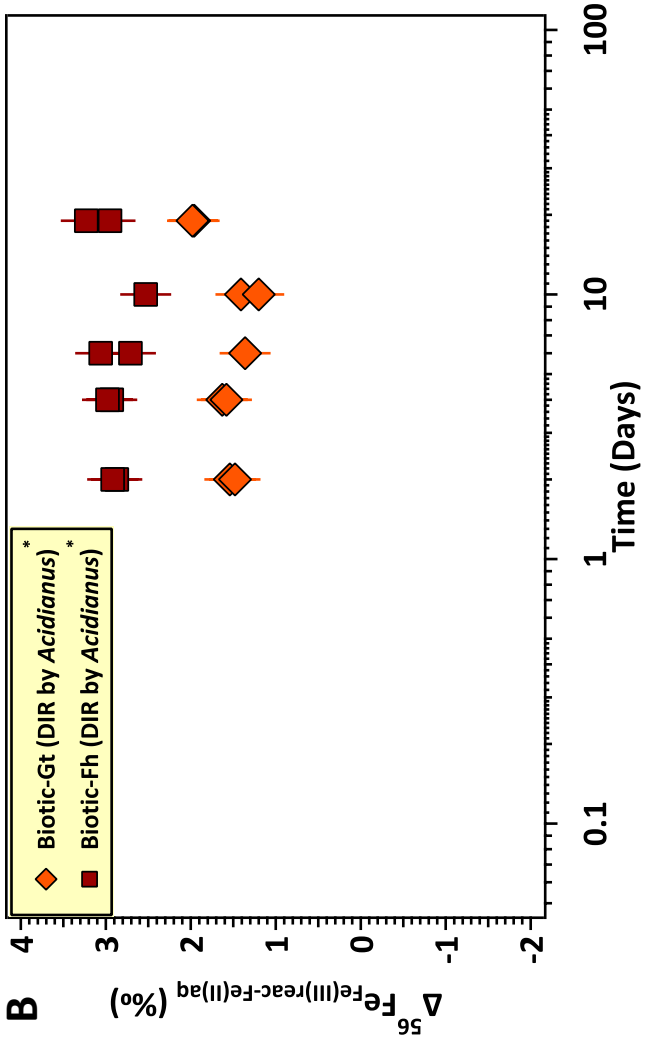
B
$\Delta^{56}Fe_{Fe(III)reac\text{-}Fe(II)aq}$ (‰)
Biotic-Gt (DIR by *Acidianus*)*
Biotic-Fh (DIR by *Acidianus*)*
Time (Days)

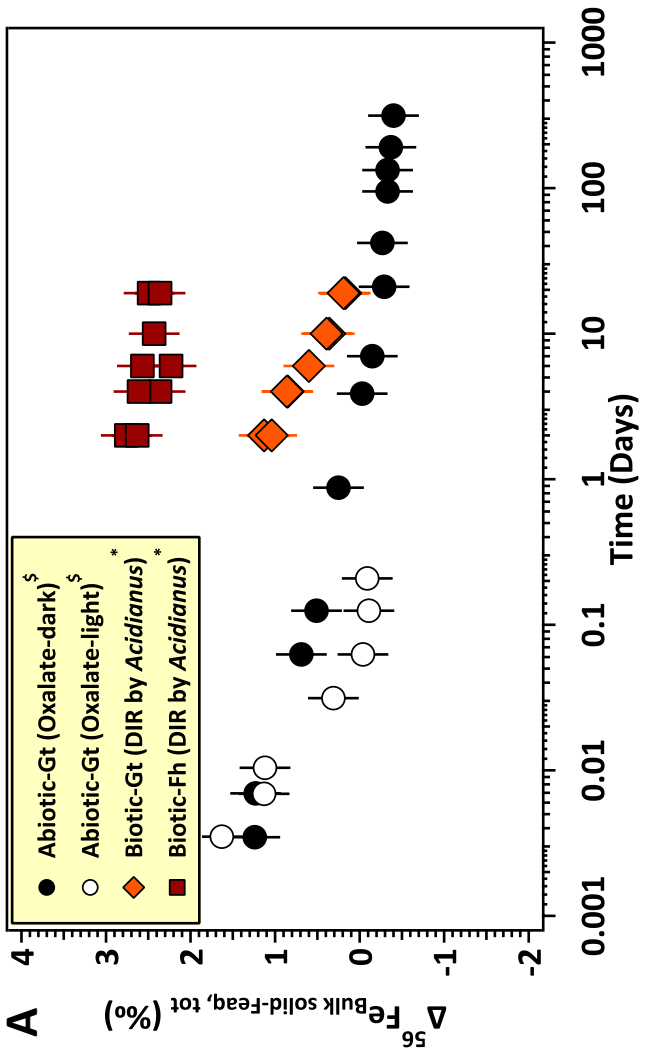
A
$\Delta^{56}Fe_{Bulk\ solid\text{-}Feag,\ tot}$ (‰)
Abiotic-Gt (Oxalate-dark)$
Abiotic-Gt (Oxalate-light)$
Biotic-Gt (DIR by *Acidianus*)*
Biotic-Fh (DIR by *Acidianus*)*
Time (Days)

Figure 9

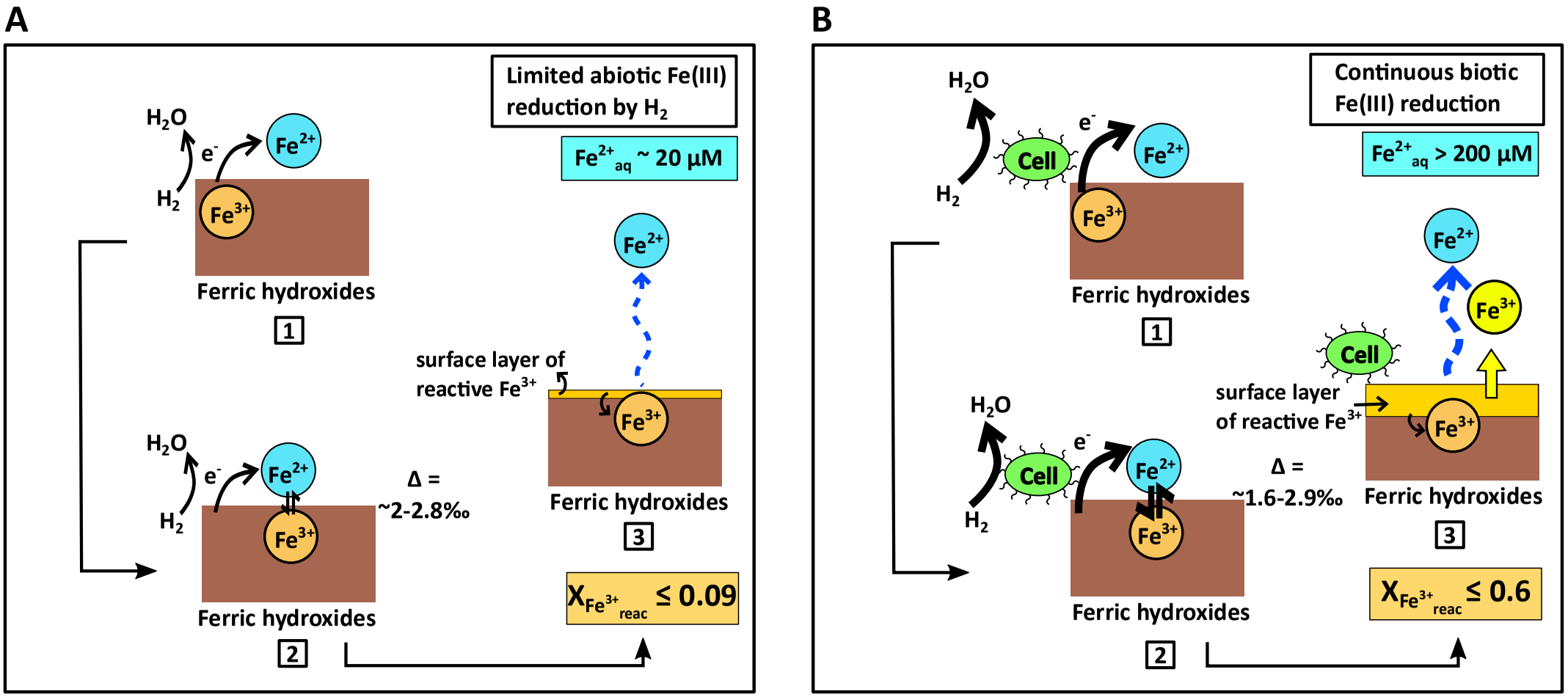

1
- a. $2Fe(OH)_3 \rightarrow 2Fe^{3+}_{aq} + 6OH^-$
- b. $H_2 \rightarrow 2H^+ + 2e^-$
- c. $2Fe^{3+}_{aq} + 2e^- \rightarrow 2Fe^{2+}_{aq}$

2
- d. $^xFe^{2+}_{aq} + {}^yFe^{3+}_{reac} \leftrightharpoons {}^yFe^{2+}_{aq} + {}^xFe^{3+}_{reac}$

Fe^{2+} Fe^{2+}_{aq}

Fe^{3+} Fe^{3+}_{reac}

Fe^{3+} Fe^{3+}_{aq}

3
- e. Release of Fe_{aq}^{2+} in the solution due to low pH
- f. Dissolution of Fe_{reac}^{3+} producing Fe_{aq}^{3+} (biotic, final stage when $X_{Fe^{3+}reac}$ is high)

Figure 10

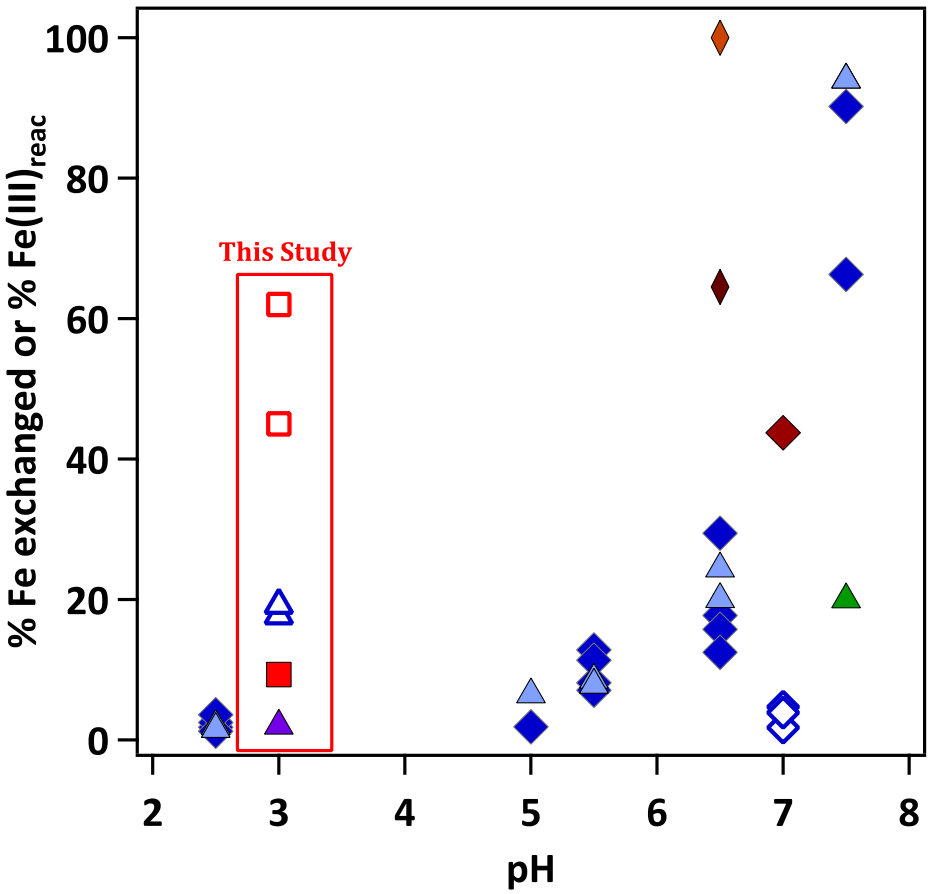

Ferrihydrite Experiments

- Fh (Biotic)*
- Fh (Abiotic)*
- Fh-dried (Abiotic)[&]
- Fh with 25 ppm DOM (Abiotic)[&]
- Fh with 150 ppm DOM (Abiotic)[&]

Fh : Ferrihydrite with SSA 300-600 m^2/g

Goethite Experiments

- η–Gt (Biotic)*
- η–Gt (Abiotic)*
- μ–Gt (Biotic)[¶, ¥]
- μ–Gt (Abiotic)[$, #, §]
- η–Gt (Abiotic)[$, #, §]
- η–Gt (Abiotic)[¢]

η–Gt : Goethite with SSA 88-119 m^2/g

μ–Gt : Goethite with SSA 40-55 m^2/g

* This Study